A triangular finite shell element based on a fully nonlinear shell formulation

Article *in* Computational Mechanics · August 2003

DOI: 10.1007/s00466-003-0458-8

CITATIONS
72

READS
562

3 authors:

Eduardo M. B. Campello
University of São Paulo
44 PUBLICATIONS **428** CITATIONS
SEE PROFILE

Paulo M Pimenta
University of São Paulo
112 PUBLICATIONS **1,096** CITATIONS
SEE PROFILE

Peter Wriggers
Leibniz Universität Hannover
939 PUBLICATIONS **18,489** CITATIONS
SEE PROFILE

Computational Mechanics 31 (2003) 505–518 © Springer-Verlag 2003
DOI 10.1007/s00466-003-0458-8

A triangular finite shell element based on a fully nonlinear shell formulation

E. M. B. Campello, P. M. Pimenta, P. Wriggers

Abstract This work presents a fully nonlinear six-parameter (3 displacements and 3 rotations) shell model for finite deformations together with a triangular shell finite element for the solution of the resulting static boundary value problem. Our approach defines energetically conjugated generalized cross-sectional stresses and strains, incorporating first-order shear deformations for an inextensible shell director (no thickness change). Finite rotations are treated by the Euler–Rodrigues formula in a very convenient way, and alternative parameterizations are also discussed herein. Condensation of the three-dimensional finite strain constitutive equations is performed by applying a mathematically consistent plane stress condition, which does not destroy the symmetry of the linearized weak form. The results are general and can be easily extended to inelastic shells once a stress integration scheme within a time step is at hand. A special displacement-based triangular shell element with 6 nodes is furthermore introduced. The element has a nonconforming linear rotation field and a compatible quadratic interpolation scheme for the displacements. Locking is not observed as the performance of the element is assessed by several numerical examples, which also illustrate the robustness of our formulation. We believe that the combination of reliable triangular shell elements with powerful mesh generators is an excellent tool for nonlinear finite element analysis.

Keywords Nonlinear shell formulation, Large strains, Finite rotations, Triangular shell element

Received: 5 December 2002 / Accepted: 20 May 2003

E. M. B. Campello, P. M. Pimenta (✉)
Polytechnic School at University of São Paulo,
P.O. Box 61548, 05424-970 São Paulo, Brazil
e-mail: ppimenta@usp.br

P. Wriggers
Institut für Baumechanik und Numerische Mechanik,
Universität Hannover, Appelstrasse 9A,
30167 Hannover, Germany

Fellowship funding from FAPESP (*Fundação de Amparo à Pesquisa do Estado de São Paulo*) and CNPq (*Conselho Nacional de Pesquisa*), together with the material support and stimulating discussions in IBNM (*Institut für Baumechanik und Numerische Mechanik*), are gratefully acknowledged in this work.

1 Introduction

Most of the research carried out over the past two decades regarding nonlinear finite shell elements deals essentially with quadrilateral elements. As a result of locking phenomena triangular domains were very often avoided, despite their greater flexibility for mesh generators. With respect to shell kinematics, a large number of these works commonly employ only two components to entirely describe the shell rotation field. The so-called drilling degree-of-freedom is frequently ignored as it has no inherent stiffness during the shell motion. Six-parameters – 3 displacements and 3 rotations – shell models can however be very convenient for engineering applications since no special connection scheme is necessary at the shell edges and intersections, and no particular care needs to be taken when coupling shell and rod elements.

In this work we review and extend the geometrically-exact six-parameter shell formulation of Pimenta [17] (which is one of the existing shell models undergoing large strains and finite rotations, see [2, 9–11, 15, 24, 32] to name just a few others), and introduce a special triangular shell finite element for the solution of the resultant static boundary value problem.

Although it may be not necessary, our approach defines energetically conjugated cross sectional stresses and strains, based on the concept of shell director with a standard Reissner–Mindlin kinematical assumption. Appealing is the fact that both the first Piola–Kirchhoff stress tensor and the deformation gradient appear as primary variables. Due to the use of cross sectional quantities, the derivation of equilibrium equations in strong and weak forms is considerably simpler, and the linearization of the latter leads naturally to a symmetric bilinear form for hyper-elastic materials and conservative loadings (even far from equilibrium states). The resulting expressions are much similar to those obtained for geometrically-exact spatial rods in [18, 19], rendering a very convenient pattern for the simultaneous coding of rod and shell finite elements.

Particular attention is drawn in deriving elastic constitutive equations from fully three-dimensional finite strain constitutive models, in a totally consistent way. A genuine plane-stress condition is enforced by vanishing the true (first Piola–Kirchhoff) mid-surface normal stress, not destroying the symmetry of the linearized weak form. This idea is general and can be easily extended to inelastic shells, once a 3-D stress integration scheme within a time step is at hand. Although the shell director is assumed to be inextensible during the motion, thickness deformation

can be straightforwardly accounted for in a multi-parameter theory (see [22]).

We assume a plane reference configuration for the shell mid-surface. Initially curved shells can then be regarded as a stress-free deformed state from this plane position, similarly as in [20] for rods. This approach prevents the use of convective non-Cartesian coordinate systems and simplifies the comprehension of tensor quantities, since only components on orthogonal frames are employed. In addition, it allows for initial strains and curvatures that are completely independent of the isoparametric concept.

Finite rotations are treated here by the Euler–Rodrigues formula in a pure Lagrangian way. Two different parameterizations are considered: (i) the usual Euler rotation vector and (ii) a family of modified Rodrigues parameters. The first is singularity-free for any rotation increment while the latter delivers computationally more efficient expressions.

A special displacement-based triangular shell element is furthermore introduced. The element has 6 nodes and is flat in the reference configuration, with a nonconforming linear rotation field and a compatible quadratic interpolation scheme for the displacements. No numerical tricks such as ANS, EAS or reduced integration with hourglass control are needed to improve its performance. Therefore, the simplicity of pure displacement-based elements is fully preserved and enjoyed here, and this constitutes one of the primary features of this work. Locking is not observed as the accuracy of the element is assessed by several numerical examples, which also illustrate the robustness of our formulation. We believe that the combination of reliable triangular shell elements with powerful mesh generators is an excellent tool for nonlinear finite element analysis.

Throughout the text, italic Latin or Greek lowercase letters $(a, b, \ldots, \alpha, \beta, \ldots)$ denote scalar quantities, bold italic Latin or Greek lowercase letters $(\boldsymbol{a}, \boldsymbol{b}, \ldots, \boldsymbol{\alpha}, \boldsymbol{\beta}, \ldots)$ denote vectors, bold italic Latin or Greek capital letters $(\boldsymbol{A}, \boldsymbol{B}, \ldots)$ denote second-order tensors, bold calligraphic Latin capital letters $(\boldsymbol{\mathscr{A}}, \boldsymbol{\mathscr{B}}, \ldots)$ denote third-order tensors and bold blackboard italic Latin capital letters $(\mathbb{A}, \mathbb{B}, \ldots)$ denote fourth-order tensors in a three-dimensional Euclidean space. Vectors and matrices built of tensor components on orthogonal frames (e.g. for computational purposes) are expressed by boldface upright Latin letters $(\mathbf{A}, \mathbf{B}, \ldots \mathbf{a}, \mathbf{b}, \ldots)$. Summation convention over repeated indices is adopted, with Greek indices ranging from 1 to 2 and Latin indices from 1 to 3.

2 Shell model

Kinematics

It is assumed that the middle surface of the shell is plane at the initial reference configuration[1]. Let $\{\boldsymbol{e}_1^r, \boldsymbol{e}_2^r, \boldsymbol{e}_3^r\}$ be an orthogonal system, with the vectors $\boldsymbol{e}_\alpha^r$ placed on the shell reference mid-plane and $\boldsymbol{e}_3^r$ normal to this plane, as shown in Fig. 1.

[1] Initially curved shells can be mapped by standard isoparametric means, or can be regarded as a stress-free deformed state from the plane initial position, as will be shown in a next work (see the ideas of [20] for rods).

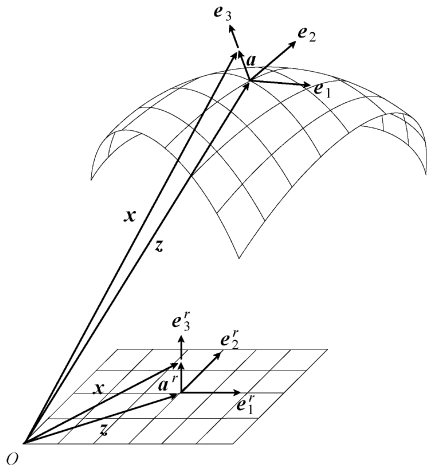

Fig. 1. Shell description and basic kinematical quantities

The position of any shell material point in the reference configuration can be described by

$$\boldsymbol{\xi} = \boldsymbol{\zeta} + \boldsymbol{a}^r \quad , \tag{1}$$

where the vector

$$\boldsymbol{\zeta} = \xi_\alpha \boldsymbol{e}_\alpha^r \tag{2}$$

defines a point on the reference mid-surface and $\boldsymbol{a}^r$ is the shell director at this point, given by

$$\boldsymbol{a}^r = \zeta \boldsymbol{e}_3^r \quad . \tag{3}$$

Here $\zeta \in H = [-h^b, h^t]$ is the thickness coordinate, with $h = h^b + h^t$ being the shell thickness in the reference configuration (observe that $\{\xi_\alpha,\ \zeta\}$ sets a three-dimensional Cartesian frame).

In the current configuration the position $\boldsymbol{x}$ of any material point can be expressed by the vector field

$$\boldsymbol{x} = \boldsymbol{z} + \boldsymbol{a} \quad , \tag{4}$$

where $\boldsymbol{z} = \hat{\boldsymbol{z}}(\xi_\alpha)$ describes the current position of a point in the middle surface and $\boldsymbol{a}$ is the current director at this point, obtained as

$$\boldsymbol{a} = \boldsymbol{Q}\boldsymbol{a}^r \quad , \tag{5}$$

with $\boldsymbol{Q}$ as the rotation tensor. Notice that no thickness change is assumed during the motion (this issue will be better discussed in Sect. 3), and that first order shear deformations are accounted for since $\boldsymbol{a}$ is not necessarily normal to the current mid-surface. We use in the text the notation $\boldsymbol{v} = \boldsymbol{Q}\boldsymbol{v}^r \Leftrightarrow \boldsymbol{v}^r = \boldsymbol{Q}^T\boldsymbol{v}$, for any vectors $\boldsymbol{v}, \boldsymbol{v}^r \in \mathbb{R}^3$. The vector $\boldsymbol{v}^r$ is said to be the back-rotated counterpart of $\boldsymbol{v}$ and is not affected by superimposed rigid body motions. Let now $\{\boldsymbol{e}_1, \boldsymbol{e}_2, \boldsymbol{e}_3\}$ be a local orthogonal system on the current configuration, with $\boldsymbol{e}_i = \boldsymbol{Q}\boldsymbol{e}_i^r$, as depicted in Fig. 1. It is easy to show that any $\boldsymbol{v}$ has the same components on the current system $\{\boldsymbol{e}_1, \boldsymbol{e}_2, \boldsymbol{e}_3\}$ as its counterpart $\boldsymbol{v}^r$ has on the reference system $\{\boldsymbol{e}_1^r, \boldsymbol{e}_2^r, \boldsymbol{e}_3^r\}$.

The rotation tensor $\boldsymbol{Q}$ may be expressed in terms of the Euler rotation vector $\boldsymbol{\theta}$, by means of the well-known Euler–Rodrigues formula

$$\boldsymbol{Q} = \boldsymbol{I} + h_1(\theta)\boldsymbol{\Theta} + h_2(\theta)\boldsymbol{\Theta}^2 \quad , \tag{6}$$

in which θ is the true rotation angle given by $\theta = \|\boldsymbol{\theta}\|$. In (6) the following trigonometric functions have been introduced:

$$h_1(\theta) = \frac{\sin\,\theta}{\theta} \quad \text{and} \quad h_2(\theta) = \frac{1}{2}\left(\frac{\sin\,\theta/2}{\theta/2}\right)^2 \ . \tag{7}$$

Still in (6) $\boldsymbol{\Theta}$ is the skew-symmetric tensor whose axial vector is $\boldsymbol{\theta}$, indicated herein by $\boldsymbol{\Theta} = \text{skew}(\boldsymbol{\theta})$. Another sort of parameterization for the rotation field, which was already employed in [21], is discussed in detail in appendix A.

Having defined $\boldsymbol{z}$ and $\boldsymbol{\zeta}$, the displacements of any point of the reference middle plane can be computed by

$$\boldsymbol{u} = \boldsymbol{z} - \boldsymbol{\zeta} \ . \tag{8}$$

The components of $\boldsymbol{u}$ and $\boldsymbol{\theta}$ on a global Cartesian system constitute the 6 degrees-of-freedom of this shell model.

Two skew-symmetric tensors that describe the specific rotations of the director can be defined as $\boldsymbol{K}_\alpha = \boldsymbol{Q}_{,\alpha}\boldsymbol{Q}^T$, where we have introduced the notation $(\bullet)_{,\alpha} = \partial(\bullet)/\partial\xi_\alpha$ for derivatives. One can show that the corresponding axial vectors are

$$\boldsymbol{\kappa}_\alpha = \text{axial}(\boldsymbol{K}_\alpha) = \boldsymbol{\Gamma}\boldsymbol{\theta}_{,\alpha} \ , \tag{9}$$

with the tensor $\boldsymbol{\Gamma}$ given by

$$\boldsymbol{\Gamma} = \boldsymbol{I} + h_2(\theta)\boldsymbol{\Theta} + h_3(\theta)\boldsymbol{\Theta}^2 \ . \tag{10}$$

In this expression, $h_2(\theta)$ was already stated in (7) while $h_3(\theta)$ is

$$h_3(\theta) = \frac{1 - h_1(\theta)}{\theta^2} \ . \tag{11}$$

We remark that the useful properties $\boldsymbol{\Gamma}^T = \boldsymbol{Q}^T\boldsymbol{\Gamma} = \boldsymbol{\Gamma}\boldsymbol{Q}^T$ and $\boldsymbol{\Gamma} = \boldsymbol{Q}^T\boldsymbol{\Gamma}\boldsymbol{Q} = \boldsymbol{Q}\boldsymbol{\Gamma}\boldsymbol{Q}^T$ hold for $\boldsymbol{\Gamma}$.

From differentiation of (4) with respect to $\boldsymbol{\xi}$ one can evaluate the deformation gradient $\boldsymbol{F}$. After some algebra one has

$$\boldsymbol{F} = \boldsymbol{Q}\left[\boldsymbol{I} + \left(\boldsymbol{\eta}^r_\alpha + \boldsymbol{\kappa}^r_\alpha \times \boldsymbol{a}^r\right) \otimes \boldsymbol{e}^r_\alpha\right] \ , \tag{12}$$

in which

$$\boldsymbol{\eta}^r_\alpha = \boldsymbol{Q}^T\boldsymbol{z}_{,\alpha} - \boldsymbol{e}^r_\alpha \quad \text{and} \quad \boldsymbol{\kappa}^r_\alpha = \boldsymbol{\Gamma}^T\boldsymbol{\theta}_{,\alpha} \ . \tag{13}$$

These two vectors may be regarded as cross-sectional generalized strains, with $\boldsymbol{z}_{,\alpha} = \boldsymbol{e}^r_\alpha + \boldsymbol{u}_{,\alpha}$ obtained from (8) and (2). One may understand that the components $\boldsymbol{\eta}^r_\alpha \cdot \boldsymbol{e}^r_\beta$ of $\boldsymbol{\eta}^r_\alpha$ operate as membrane strains, while $\boldsymbol{\eta}^r_\alpha \cdot \boldsymbol{e}^r_3$ as transversal shear strains. Expressions (13) are the back-rotated counterparts of $\boldsymbol{\eta}_\alpha = \boldsymbol{z}_{,\alpha} - \boldsymbol{e}_\alpha$ and (9), respectively.

Introducing the strain vectors

$$\boldsymbol{\gamma}^r_\alpha = \boldsymbol{\eta}^r_\alpha + \boldsymbol{\kappa}^r_\alpha \times \boldsymbol{a}^r \tag{14}$$

in (12), the deformation gradient may be rewritten as

$$\boldsymbol{F} = \boldsymbol{Q}\boldsymbol{F}^r \ , \tag{15}$$

where $\boldsymbol{F}^r$ is called the back-rotated deformation gradient and is given by

$$\boldsymbol{F}^r = \boldsymbol{I} + \boldsymbol{\gamma}^r_\alpha \otimes \boldsymbol{e}^r_\alpha \ . \tag{16}$$

Differentiation of (15) with respect to time (denoted by a superposed dot) renders the velocity gradient as follows

$$\dot{\boldsymbol{F}} = \boldsymbol{\Omega}\boldsymbol{F} + \boldsymbol{Q}\left(\dot{\boldsymbol{\gamma}}^r_\alpha \otimes \boldsymbol{e}^r_\alpha\right) \ , \tag{17}$$

where the skew-symmetric tensor $\boldsymbol{\Omega} = \dot{\boldsymbol{Q}}\boldsymbol{Q}^T$ represents the director spin. Its axial vector is denoted by $\boldsymbol{\omega} = \text{axial}(\boldsymbol{\Omega})$ and similarly to (9) is obtained as

$$\boldsymbol{\omega} = \boldsymbol{\Gamma}\dot{\boldsymbol{\theta}} \ . \tag{18}$$

In order to fully evaluate expression (17), the time derivatives $\dot{\boldsymbol{\gamma}}^r_\alpha$ are needed. With the aid of the identity $(\dot{\boldsymbol{Q}})_{,\alpha} = (\dot{\boldsymbol{Q}}_{,\alpha})$ it is possible to arrive at $\boldsymbol{\Omega}_{,\alpha} = \dot{\boldsymbol{K}}_\alpha - \boldsymbol{\Omega}\boldsymbol{K}_\alpha + \boldsymbol{K}_\alpha\boldsymbol{\Omega}$, or equivalently

$$\boldsymbol{\omega}_{,\alpha} = \dot{\boldsymbol{\kappa}}_\alpha - \boldsymbol{\omega} \times \boldsymbol{\kappa}_\alpha \ , \tag{19}$$

from which after some algebra one has

$$\dot{\boldsymbol{\kappa}}^r_\alpha = \boldsymbol{Q}^T\boldsymbol{\omega}_{,\alpha} \ . \tag{20}$$

Then, having the expressions for $\dot{\boldsymbol{\kappa}}^r_\alpha$, from (14) one can write

$$\dot{\boldsymbol{\gamma}}^r_\alpha = \dot{\boldsymbol{\eta}}^r_\alpha + \dot{\boldsymbol{\kappa}}^r_\alpha \times \boldsymbol{a}^r \ , \tag{21}$$

where

$$\dot{\boldsymbol{\eta}}^r_\alpha = \boldsymbol{Q}^T\left(\dot{\boldsymbol{u}}_{,\alpha} + \boldsymbol{Z}_{,\alpha}\boldsymbol{\Gamma}\dot{\boldsymbol{\theta}}\right) \quad \text{and} \quad \dot{\boldsymbol{\kappa}}^r_\alpha = \boldsymbol{Q}^T\left(\boldsymbol{\Gamma}_{,\alpha}\dot{\boldsymbol{\theta}} + \boldsymbol{\Gamma}\dot{\boldsymbol{\theta}}_{,\alpha}\right) \ . \tag{22}$$

Here the skew-symmetric tensors $\boldsymbol{Z}_{,\alpha} = \text{skew}\left(\boldsymbol{z}_{,\alpha}\right)$ and the derivatives

$$\begin{aligned}\boldsymbol{\Gamma}_{,\alpha} = {} & h_2(\theta)\boldsymbol{\Theta}_{,\alpha} + h_3(\theta)\left(\boldsymbol{\Theta}\boldsymbol{\Theta}_{,\alpha} + \boldsymbol{\Theta}_{,\alpha}\boldsymbol{\Theta}\right) \\ & + h_4(\theta)\left(\boldsymbol{\theta}\cdot\boldsymbol{\theta}_{,\alpha}\right)\boldsymbol{\Theta} + h_5(\theta)\left(\boldsymbol{\theta}\cdot\boldsymbol{\theta}_{,\alpha}\right)\boldsymbol{\Theta}^2\end{aligned} \tag{23}$$

have been introduced. Property (20) was employed in deriving $(22)_2$. In turn, in (23) $\boldsymbol{\Theta}_{,\alpha} = \text{skew}\left(\boldsymbol{\theta}_{,\alpha}\right)$ are two skew-symmetric tensors, and

$$h_4(\theta) = \frac{h_1(\theta) - 2h_2(\theta)}{\theta^2} \quad \text{and} \quad h_5(\theta) = \frac{h_2(\theta) - 3h_3(\theta)}{\theta^2} \tag{24}$$

are two additional trigonometric functions.

Statics

Let the first Piola-Kirchhoff stress tensor be written as

$$\boldsymbol{P} = \boldsymbol{Q}\boldsymbol{P}^r \ , \tag{25}$$

where $\boldsymbol{P}^r$ is called the back-rotated first Piola–Kirchhoff stress tensor, herein expressed by

$$\boldsymbol{P}^r = \boldsymbol{\tau}^r_i \otimes \boldsymbol{e}^r_i \ . \tag{26}$$

The quantities $\boldsymbol{\tau}^r_i$ are back-rotated stress vectors, and act on cross-sectional planes whose normals on the reference configuration are $\boldsymbol{e}^r_i$. Integration of these stress vectors along the shell thickness allows the definition of generalized cross-sectional stresses, i.e.

$$\boldsymbol{n}^r_\alpha = \int_H \boldsymbol{\tau}^r_\alpha \,\mathrm{d}\zeta \quad \text{and} \quad \boldsymbol{m}^r_\alpha = \int_H \boldsymbol{a}^r \times \boldsymbol{\tau}^r_\alpha \,\mathrm{d}\zeta \ . \tag{27}$$

In this case $\boldsymbol{n}^r_\alpha$ are said to be the back-rotated cross sectional forces and $\boldsymbol{m}^r_\alpha$ the back-rotated cross sectional moments, both per unit length.

Knowing the expressions of $\boldsymbol{P}$ and $\dot{\boldsymbol{F}}$, it is not difficult to show that the shell internal power per unit reference volume may be written as

$$\boldsymbol{P} : \dot{\boldsymbol{F}} = \boldsymbol{\tau}_\alpha^r \cdot \dot{\boldsymbol{\gamma}}_\alpha^r \ , \tag{28}$$

where the property $\boldsymbol{P}\boldsymbol{F}^T : \boldsymbol{\Omega} = 0$, arising from the local moment balance, needs to be used. If one introduces (21) in (28) and performs some manipulation with the cross product it renders

$$\boldsymbol{\tau}_\alpha^r \cdot \dot{\boldsymbol{\gamma}}_\alpha^r = \boldsymbol{\tau}_\alpha^r \cdot \dot{\boldsymbol{\eta}}_\alpha^r + \left(\boldsymbol{a}^r \times \boldsymbol{\tau}_\alpha^r\right) \cdot \dot{\boldsymbol{\kappa}}_\alpha^r \ . \tag{29}$$

Notice that the stress vector $\boldsymbol{\tau}_3^r$ remains powerless, as should be expected for a rigid shell director (recall that no thickness stretching is assumed). Integration of (29) over the thickness along with definitions (27) provides

$$\int_H \boldsymbol{\tau}_\alpha^r \cdot \dot{\boldsymbol{\gamma}}_\alpha^r \, \mathrm{d}\zeta = \boldsymbol{n}_\alpha^r \cdot \dot{\boldsymbol{\eta}}_\alpha^r + \boldsymbol{m}_\alpha^r \cdot \dot{\boldsymbol{\kappa}}_\alpha^r \ . \tag{30}$$

We remark that the vectors $\boldsymbol{\tau}_\alpha^r$, $\boldsymbol{\gamma}_\alpha^r$, $\boldsymbol{n}_\alpha^r$, $\boldsymbol{m}_\alpha^r$, $\boldsymbol{\eta}_\alpha^r$ and $\boldsymbol{\kappa}_\alpha^r$ are not affected by superimposed rigid body motions. Collecting the shell cross-sectional quantities in the 3 vectors displayed below

$$\boldsymbol{\sigma}_\alpha = \begin{bmatrix} \boldsymbol{n}_\alpha^r \\ \boldsymbol{m}_\alpha^r \end{bmatrix}, \quad \boldsymbol{\varepsilon}_\alpha = \begin{bmatrix} \boldsymbol{\eta}_\alpha^r \\ \boldsymbol{\kappa}_\alpha^r \end{bmatrix} \quad \text{and} \quad \boldsymbol{d} = \begin{bmatrix} \boldsymbol{u} \\ \boldsymbol{\theta} \end{bmatrix} \ , \tag{31}$$

then (30) may be restated as follows

$$\int_H \boldsymbol{\tau}_\alpha^r \cdot \dot{\boldsymbol{\gamma}}_\alpha^r \, \mathrm{d}\zeta = \boldsymbol{\sigma}_\alpha \cdot \dot{\boldsymbol{\varepsilon}}_\alpha \ . \tag{32}$$

In this expression, the time derivative $\dot{\boldsymbol{\varepsilon}}_\alpha$ (consisting of the components $\dot{\boldsymbol{\eta}}_\alpha^r$ and $\dot{\boldsymbol{\kappa}}_\alpha^r$) may be written in a very compact manner as

$$\dot{\boldsymbol{\varepsilon}}_\alpha = \boldsymbol{\Psi}_\alpha \dot{\boldsymbol{d}} \ , \tag{33}$$

in which the operator $\boldsymbol{\Psi}_\alpha$ emanates from (22) and is

$$\boldsymbol{\Psi}_\alpha = \begin{bmatrix} \boldsymbol{Q}^T & \boldsymbol{O} \\ \boldsymbol{O} & \boldsymbol{Q}^T \end{bmatrix} \begin{bmatrix} \boldsymbol{I} & \boldsymbol{O} & \boldsymbol{Z}_{,\alpha}\boldsymbol{\Gamma} \\ \boldsymbol{O} & \boldsymbol{\Gamma} & \boldsymbol{\Gamma}_{,\alpha} \end{bmatrix} \boldsymbol{\Delta}_\alpha \quad (\text{no sum}) \ , \tag{34}$$

with

$$\boldsymbol{\Delta}_\alpha = \begin{bmatrix} \boldsymbol{I}\frac{\partial}{\partial \xi_\alpha} & \boldsymbol{O} \\ \boldsymbol{O} & \boldsymbol{I}\frac{\partial}{\partial \xi_\alpha} \\ \boldsymbol{O} & \boldsymbol{I} \end{bmatrix} \ . \tag{35}$$

Using (32), the shell internal power on a domain $\Omega \subset \mathbb{R}^2$ is then given by

$$P_{\text{int}} = \int_\Omega \boldsymbol{\sigma}_\alpha \cdot \dot{\boldsymbol{\varepsilon}}_\alpha \, \mathrm{d}\Omega \ . \tag{36}$$

On the other hand, if one defines a vector $\boldsymbol{t}$ as the surface traction per unit reference area, and another vector $\boldsymbol{b}$ as the body force per unit reference volume, the shell external power on the same domain $\Omega \subset \mathbb{R}^2$ can be expressed by

$$P_{\text{ext}} = \int_\Omega \left[\boldsymbol{t}^t \cdot \dot{\boldsymbol{x}}^t + \boldsymbol{t}^b \cdot \dot{\boldsymbol{x}}^b + \int_H \boldsymbol{b} \cdot \dot{\boldsymbol{x}} \, \mathrm{d}\zeta \right] \mathrm{d}\Omega \ , \tag{37}$$

where $\dot{\boldsymbol{x}}$ is obtained by time differentiation of (4), i.e.

$$\dot{\boldsymbol{x}} = \dot{\boldsymbol{u}} + \boldsymbol{\omega} \times \boldsymbol{a} \ . \tag{38}$$

Introducing (18) in (38) and this in (37) one obtains

$$P_{\text{ext}} = \int_\Omega \bar{\boldsymbol{q}} \cdot \dot{\boldsymbol{d}} \, \mathrm{d}\Omega \ , \tag{39}$$

in which

$$\bar{\boldsymbol{q}} = \begin{bmatrix} \bar{\boldsymbol{n}} \\ \boldsymbol{\Gamma}^T \bar{\boldsymbol{m}} \end{bmatrix} \tag{40}$$

is defined as the vector of generalized external forces. In this case the vectors

$$\begin{aligned} \bar{\boldsymbol{n}} &= \boldsymbol{t}^t + \boldsymbol{t}^b + \int_H \boldsymbol{b} \, \mathrm{d}\zeta \quad \text{and} \\ \bar{\boldsymbol{m}} &= \boldsymbol{a}^t \times \boldsymbol{t}^t + \boldsymbol{a}^b \times \boldsymbol{t}^b + \int_H \boldsymbol{a} \times \boldsymbol{b} \, \mathrm{d}\zeta \end{aligned} \tag{41}$$

of (40) are the applied external forces and moments respectively, both per unit area of the middle surface in the reference configuration.

Remark 1
The vector

$$\bar{\boldsymbol{\mu}} = \boldsymbol{\Gamma}^T \bar{\boldsymbol{m}} \tag{42}$$

emerging from (40) is the distributed external moment truly power-conjugated with $\boldsymbol{\theta}$, and not purely $\bar{\boldsymbol{m}}$ as one would expect. The same holds for external concentrated moments. This fact has far-reaching consequences in the nonlinear analysis of structures with rotational degrees of freedom, since a non-trivial geometric contribution of the applied moments is introduced in the tangent bilinear form (see appendix C for detailed expressions).

Weak forms
In the same way as to obtain (36), one can have the expression for the shell internal virtual work on a domain $\Omega \subset \mathbb{R}^2$ as follows

$$\delta W_{\text{int}} = \int_\Omega \boldsymbol{\sigma}_\alpha \cdot \delta \boldsymbol{\varepsilon}_\alpha \, \mathrm{d}\Omega \ , \tag{43}$$

with

$$\delta \boldsymbol{\varepsilon}_\alpha = \boldsymbol{\Psi}_\alpha \delta \boldsymbol{d} \ . \tag{44}$$

The external virtual work on the same domain $\Omega \subset \mathbb{R}^2$ may be evaluated similarly to (39), i.e.

$$\delta W_{\text{ext}} = \int_\Omega \bar{\boldsymbol{q}} \cdot \delta \boldsymbol{d} \, \mathrm{d}\Omega \ , \tag{45}$$

so that the shell local equilibrium can be stated by means of the virtual work theorem in a standard way:

$$\delta W = \delta W_{\text{int}} - \delta W_{\text{ext}} = 0 \quad \text{in } \Omega, \ \forall \, \delta \boldsymbol{d} \ . \tag{46}$$

Substituting (43) and (45) in this expression and performing partial integration on the terms with $\delta \boldsymbol{u}_{,\alpha}$ and

$(\boldsymbol{\Gamma}\delta\boldsymbol{\theta})_{,\alpha}$, the following local equilibrium equations in Ω are obtained by the fundamental lemma of variational calculus

$$\begin{aligned} &\boldsymbol{n}_{\alpha,\alpha}+\bar{\boldsymbol{n}}=\boldsymbol{o} \quad \text{and} \\ &\boldsymbol{m}_{\alpha,\alpha}+\boldsymbol{z}_{,\alpha}\times\boldsymbol{n}_{\alpha}+\bar{\boldsymbol{m}}=\boldsymbol{o}\ . \end{aligned} \tag{47}$$

Here the cross-sectional resultants

$$\boldsymbol{n}_{\alpha}=\boldsymbol{Q}\boldsymbol{n}^{r}_{\alpha} \quad \text{and} \quad \boldsymbol{m}_{\alpha}=\boldsymbol{Q}\boldsymbol{m}^{r}_{\alpha} \tag{48}$$

have been introduced with respect to the current configuration. Equilibrium equations (47) can be directly attained by Statics as well.

The Gateaux derivative of (46) with respect to $\boldsymbol{d}$ leads to the tangent bilinear form

$$\begin{aligned} \delta^{*}(\delta W)=&\int_{\Omega}(\boldsymbol{\Psi}_{\alpha}\delta\boldsymbol{d})\cdot\left(\boldsymbol{D}_{\alpha\beta}\boldsymbol{\Psi}_{\beta}\delta^{*}\boldsymbol{d}\right)\mathrm{d}\Omega \\ &+\int_{\Omega}(\boldsymbol{\Lambda}_{\alpha}\delta\boldsymbol{d})\cdot(\boldsymbol{G}_{\alpha}\boldsymbol{\Lambda}_{\alpha}\delta^{*}\boldsymbol{d})\mathrm{d}\Omega-\int_{\Omega}(\delta\boldsymbol{d}\cdot\boldsymbol{L}\delta^{*}\boldsymbol{d})\mathrm{d}\Omega\ , \end{aligned} \tag{49}$$

in which the matrices $\boldsymbol{D}_{\alpha\beta}$, $\boldsymbol{G}_{\alpha}$ and $\boldsymbol{L}$ are given by

$$\boldsymbol{D}_{\alpha\beta}=\frac{\partial\boldsymbol{\sigma}_{\alpha}}{\partial\boldsymbol{\varepsilon}_{\beta}}=\begin{bmatrix}\frac{\partial\boldsymbol{n}^{r}_{\alpha}}{\partial\boldsymbol{\eta}^{r}_{\beta}} & \frac{\partial\boldsymbol{n}^{r}_{\alpha}}{\partial\boldsymbol{\kappa}^{r}_{\beta}}\\ \frac{\partial\boldsymbol{m}^{r}_{\alpha}}{\partial\boldsymbol{\eta}^{r}_{\beta}} & \frac{\partial\boldsymbol{m}^{r}_{\alpha}}{\partial\boldsymbol{\kappa}^{r}_{\beta}}\end{bmatrix},$$

$$\boldsymbol{G}_{\alpha}=\begin{bmatrix}\boldsymbol{O} & \boldsymbol{O} & \boldsymbol{G}^{u'\theta}_{\alpha}\\ \boldsymbol{O} & \boldsymbol{O} & \boldsymbol{G}^{\theta'\theta}_{\alpha}\\ \boldsymbol{G}^{\theta u'}_{\alpha} & \boldsymbol{G}^{\theta\theta'}_{\alpha} & \boldsymbol{G}^{\theta\theta}_{\alpha}\end{bmatrix} \quad \text{and} \tag{50}$$

$$\boldsymbol{L}=\frac{\partial\bar{\boldsymbol{q}}}{\partial\boldsymbol{d}}=\begin{bmatrix}\frac{\partial\bar{\boldsymbol{n}}}{\partial\boldsymbol{u}} & \frac{\partial\bar{\boldsymbol{n}}}{\partial\boldsymbol{\theta}}\\ \frac{\partial\bar{\boldsymbol{\mu}}}{\partial\boldsymbol{u}} & \frac{\partial\bar{\boldsymbol{\mu}}}{\partial\boldsymbol{\theta}}\end{bmatrix}\ .$$

The sub-matrices of $\boldsymbol{G}_{\alpha}$ are stated in appendix B and were firstly presented in [17]. They are functions of $\boldsymbol{\sigma}_{\alpha}$ and $\boldsymbol{d}$ and remain always symmetric, even far from equilibrium states. The sub-matrices of $\boldsymbol{L}$, however, depend on the character of the external load as one can see in $(50)_3$ (some expressions can be found in appendix C). Therefore the bilinear form (49) is symmetric whenever

$$\boldsymbol{D}_{\alpha\beta}=\boldsymbol{D}^{T}_{\beta\alpha} \quad \text{and} \quad \boldsymbol{L}=\boldsymbol{L}^{T}\ , \tag{51}$$

i.e., whenever the material is hyper-elastic and the external loading is locally conservative, respectively.

Let us introduce now the following shell tangent tensors

$$\frac{\partial\boldsymbol{\tau}^{r}_{\alpha}}{\partial\boldsymbol{\gamma}^{r}_{\beta}}=\bar{\boldsymbol{C}}_{\alpha\beta} \tag{52}$$

and the following derivatives

$$\frac{\partial\boldsymbol{\gamma}^{r}_{\gamma}}{\partial\boldsymbol{\eta}^{r}_{\beta}}=\delta_{\gamma\beta}\boldsymbol{I} \quad \text{and} \quad \frac{\partial\boldsymbol{\gamma}^{r}_{\gamma}}{\partial\boldsymbol{\kappa}^{r}_{\beta}}=-\delta_{\gamma\beta}\boldsymbol{A}^{r}\ , \tag{53}$$

where $\delta_{\alpha\beta}$ is the Kronecker symbol and $\boldsymbol{A}^{r}=\mathrm{skew}(\boldsymbol{a}^{r})$. The sub-matrices of $\boldsymbol{D}_{\alpha\beta}$ in $(50)_1$ can then be computed by the chain rule as

$$\begin{aligned} &\frac{\partial\boldsymbol{n}^{r}_{\alpha}}{\partial\boldsymbol{\eta}^{r}_{\beta}}=\int_{h}\bar{\boldsymbol{C}}_{\alpha\beta}\,\mathrm{d}\zeta, \quad \frac{\partial\boldsymbol{n}^{r}_{\alpha}}{\partial\boldsymbol{\kappa}^{r}_{\beta}}=-\int_{h}\bar{\boldsymbol{C}}_{\alpha\beta}\boldsymbol{A}^{r}\,\mathrm{d}\zeta, \\ &\frac{\partial\boldsymbol{m}^{r}_{\alpha}}{\partial\boldsymbol{\eta}^{r}_{\beta}}=\int_{h}\boldsymbol{A}^{r}\bar{\boldsymbol{C}}_{\alpha\beta}\,\mathrm{d}\zeta \quad \text{and} \quad \frac{\partial\boldsymbol{m}^{r}_{\alpha}}{\partial\boldsymbol{\kappa}^{r}_{\beta}}=-\int_{h}\boldsymbol{A}^{r}\bar{\boldsymbol{C}}_{\alpha\beta}\boldsymbol{A}^{r}\,\mathrm{d}\zeta\ . \end{aligned} \tag{54}$$

Notice here that $(51)_1$ is true if there exists a specific strain energy function $\psi=\psi(\boldsymbol{\gamma}^{r}_{\alpha})$ or if $\bar{\boldsymbol{C}}_{\alpha\beta}=\bar{\boldsymbol{C}}^{T}_{\beta\alpha}$.

3 Elastic constitutive equations

The plane-stress condition

Constitutive relations within this shell model can be stated to a wider range of problems if the expression (16) for $\boldsymbol{F}^{r}$ is replaced by

$$\boldsymbol{F}^{r}=\boldsymbol{I}+\boldsymbol{\gamma}^{r}_{\alpha}\otimes\boldsymbol{e}^{r}_{\alpha}+\gamma_{33}\boldsymbol{e}^{r}_{3}\otimes\boldsymbol{e}^{r}_{3}\ . \tag{55}$$

The element γ_{33} was introduced above in order to allow for transversal through-the-thickness strains. It can be regarded as an additional degree-of-freedom, which can be eliminated at the constitutive level by enforcing a plane-stress condition (a complete multi-parameter shell formulation in which γ_{33} is retained will be found in [22]). Here, a mathematically consistent plane-stress situation may be attained in which the true (first Piola–Kirchhoff) mid-surface normal stress vanishes, i.e. $\left(\boldsymbol{P}\boldsymbol{e}^{r}_{3}\right)\cdot\boldsymbol{e}_{3}=0$, rendering

$$\tau^{r}_{33}=\boldsymbol{\tau}^{r}_{3}\cdot\boldsymbol{e}^{r}_{3}=\boldsymbol{e}^{r}_{3}\cdot\boldsymbol{P}^{r}\boldsymbol{e}^{r}_{3}=0\ . \tag{56}$$

In other words, the projection of the *real* stress $\boldsymbol{P}\boldsymbol{e}^{r}_{3}$ on the *current* director $\boldsymbol{a}=\zeta\boldsymbol{e}_{3}$ is assumed to be zero, what means that τ^{r}_{33} is powerless as in (28).

Once the expression for $\boldsymbol{F}^{r}$ was modified, we introduce the following new tangent quantities

$$\frac{\partial\boldsymbol{\tau}^{r}_{\alpha}}{\partial\boldsymbol{\gamma}^{r}_{\beta}}=\boldsymbol{C}_{\alpha\beta}, \quad \frac{\partial\boldsymbol{\tau}^{r}_{\alpha}}{\partial\gamma_{33}}=\frac{\partial\tau^{r}_{33}}{\partial\boldsymbol{\gamma}^{r}_{\alpha}}=\boldsymbol{c}_{\alpha} \quad \text{and} \quad \frac{\partial\tau^{r}_{33}}{\partial\gamma_{33}}=c\ . \tag{57}$$

Condition (56) generates a nonlinear equation in γ_{33} that can be iteratively solved by the Newton Method as follows

$$\gamma^{k+1}_{33}=\gamma^{k}_{33}-\frac{1}{c\left(\gamma^{k}_{33}\right)}\tau^{r}_{33}\left(\gamma^{k}_{33}\right), \quad k=0,1,2,\ldots\ , \quad \gamma^{0}_{33}=0\ , \tag{58}$$

in which $c(\gamma_{33})$ is given by $(57)_3$. This way, γ_{33} is consistently eliminated from the shell kinematics, and the tangent tensors $\bar{\boldsymbol{C}}_{\alpha\beta}$ of (52) can be computed by means of

$$\bar{\boldsymbol{C}}_{\alpha\beta}=\boldsymbol{C}_{\alpha\beta}-\frac{1}{c}\boldsymbol{c}_{\alpha}\otimes\boldsymbol{c}_{\beta}\ . \tag{59}$$

General elastic materials

We write the symmetric Green–Lagrange strain tensor as

$$\boldsymbol{E}=\frac{1}{2}\left(\boldsymbol{F}^{T}\boldsymbol{F}-\boldsymbol{I}\right)=\frac{1}{2}\left(\boldsymbol{F}^{rT}\boldsymbol{F}^{r}-\boldsymbol{I}\right)\ , \tag{60}$$

with its energetically conjugated second Piola-Kirchhoff stress tensor $\boldsymbol{S}$ such that

$$\boldsymbol{P} = \boldsymbol{F}\boldsymbol{S} \ . \tag{61}$$

One can show that

$$\boldsymbol{P}^r = \boldsymbol{F}^r\boldsymbol{S} \tag{62}$$

also holds. A general hyper-elastic material can be fully described by a specific strain energy function $\psi = \psi(\boldsymbol{E})$, such that the second Piola–Kirchhoff stress tensor is given by

$$\boldsymbol{S} = \frac{\partial \psi}{\partial \boldsymbol{E}} \ . \tag{63}$$

As a consequence, a fourth-order tensor of elastic tangent moduli for the pair $\{\boldsymbol{S}, \boldsymbol{E}\}$ can be defined as

$$\mathbb{D} = \frac{\partial \boldsymbol{S}}{\partial \boldsymbol{E}} = \frac{\partial^2 \psi}{\partial \boldsymbol{E}^2} \ . \tag{64}$$

With the aid of the following third- and second-order tensors

$$\mathscr{B}_\alpha = \frac{\partial \boldsymbol{E}}{\partial \boldsymbol{\gamma}^r_\alpha} \quad \text{and} \quad \boldsymbol{B} = \frac{\partial \boldsymbol{E}}{\partial \gamma_{33}} \ , \tag{65}$$

the relations

$$\boldsymbol{\tau}^r_\alpha = \mathscr{B}^T_\alpha \boldsymbol{S} \quad \text{and} \quad \tau^r_{33} = \boldsymbol{B} : \boldsymbol{S} \tag{66}$$

can be readily derived. From (57), (64), (65) and (66) we arrive at

$$\begin{aligned} &\boldsymbol{C}_{\alpha\beta} = \mathscr{B}^T_\alpha \mathbb{D} \mathscr{B}_\beta + \left(\boldsymbol{e}^r_\alpha \cdot \boldsymbol{S}\boldsymbol{e}^r_\beta\right)\boldsymbol{I}, \\ &\boldsymbol{c}_\alpha = \mathscr{B}^T_\alpha \mathbb{D}\boldsymbol{B} + \left(\boldsymbol{e}^r_\alpha \cdot \boldsymbol{S}\boldsymbol{e}^r_3\right)\boldsymbol{e}^r_3 \quad \text{and} \\ &c = \boldsymbol{B} : \mathbb{D}\boldsymbol{B} + \boldsymbol{e}^r_3 \cdot \boldsymbol{S}\boldsymbol{e}^r_3 \ . \end{aligned} \tag{67}$$

The Introduction of these quantities into (59) yields tangent tensors $\bar{\boldsymbol{C}}_{\alpha\beta}$ of (52).

Remark 2

The just developed approach to ensure a mathematically consistent plane-stress condition is general, and can be straightforwardly extended to inelastic shells once a stress integration scheme within a time step is available.

Isotropic materials

When the material is in addition isotropic, the strain energy function ψ can be written as a function of the invariants of the right Cauchy–Green strain tensor $\boldsymbol{C} = \boldsymbol{F}^T\boldsymbol{F} = \boldsymbol{F}^{rT}\boldsymbol{F}^r$. We adopt here the following set of invariants

$$I_1 = \boldsymbol{I} : \boldsymbol{C}, \quad I_2 = \frac{1}{2}\boldsymbol{I} : \boldsymbol{C}^2 \quad \text{and} \quad J = \det \boldsymbol{F} \ , \tag{68}$$

with which we write $\psi = \psi(I_1, I_2, J)$. Doing so, the back-rotated first Piola–Kirchhoff stress tensor can be expressed by

$$\boldsymbol{P}^r = \frac{\partial \psi}{\partial J} J \boldsymbol{F}^{r-T} + 2\boldsymbol{F}^r \left(\frac{\partial \psi}{\partial I_1}\boldsymbol{I} + \frac{\partial \psi}{\partial I_2}\boldsymbol{C}\right) \ , \tag{69}$$

where the Jacobian J is (using the components $\gamma_{\alpha i} = \boldsymbol{\gamma}^r_\alpha \cdot \boldsymbol{e}^r_i$ of $\boldsymbol{\gamma}^r_\alpha$)

$$\begin{aligned} &J = (1+\gamma_{33})\bar{J}, \quad \text{with} \\ &\bar{J} = (1+\gamma_{11})(1+\gamma_{22}) - \gamma_{12}\gamma_{21} \ , \end{aligned} \tag{70}$$

and where $\boldsymbol{F}^r$ and $\boldsymbol{F}^{r-T}$ can be stated explicitly by (55) and

$$\boldsymbol{F}^{r-T} = \frac{1}{\bar{J}} \begin{bmatrix} 1+\gamma_{22} & -\gamma_{12} & \frac{\gamma_{12}\gamma_{23} - \gamma_{13}(1+\gamma_{22})}{1+\gamma_{33}} \\ -\gamma_{21} & 1+\gamma_{11} & \frac{\gamma_{21}\gamma_{13} - \gamma_{23}(1+\gamma_{11})}{1+\gamma_{33}} \\ 0 & 0 & \frac{\bar{J}}{1+\gamma_{33}} \end{bmatrix} \ . \tag{71}$$

From the plane stress condition (56) and from (69) one thus has

$$\begin{aligned} &\frac{\partial \psi}{\partial J}\bar{J} + 2\left(\frac{\partial \psi}{\partial I_1} + \frac{\partial \psi}{\partial I_2}\gamma_{\alpha 3}\gamma_{\alpha 3}\right)(1+\gamma_{33}) \\ &\quad + 2\frac{\partial \psi}{\partial I_2}(1+\gamma_{33})^3 = 0 \ . \end{aligned} \tag{72}$$

Depending on the character of ψ it is possible to find an analytical solution for this equation, circumventing the Newton iterations of (58). This is the case of the simple poly-convex neo-Hookean material defined by

$$\psi(I_1, J) = \frac{1}{2}\lambda\left(\frac{1}{2}\left(J^2 - 1\right) - \ln J\right) + \frac{1}{2}\mu(I_1 - 3 - 2\ln J) \ , \tag{73}$$

proposed by Simo in [25], where the Lame constants λ and μ are material parameters. Substituting (73) into (72) one arrives after some algebra at

$$(1+\gamma_{33})^2 = \frac{\lambda + 2\mu}{\lambda\bar{J}^2 + 2\mu} \ , \tag{74}$$

which means that the transversal (through-the-thickness) strain for this particular material is given by

$$\gamma_{33} = \sqrt{\frac{\lambda + 2\mu}{\lambda\bar{J}^2 + 2\mu}} - 1 \ . \tag{75}$$

Furthermore, introducing (73) into (69) leads to the expression for the back-rotated first Piola-Kirchhoff stress tensor

$$\boldsymbol{P}^r = \boldsymbol{\tau}^r_i \otimes \boldsymbol{e}^r_i = \left(\frac{1}{2}\lambda\left(J^2 - 1\right) - \mu\right)\boldsymbol{F}^{r-T} + \mu\boldsymbol{F}^r \ , \tag{76}$$

from which, together with (74), we get

$$\begin{aligned} \boldsymbol{\tau}^r_1 &= \mu\vartheta \begin{bmatrix} 1+\gamma_{22} \\ -\gamma_{21} \\ 0 \end{bmatrix} + \mu \begin{bmatrix} \gamma_{11} - \gamma_{22} \\ \gamma_{12} + \gamma_{21} \\ \gamma_{13} \end{bmatrix} \quad \text{and} \\ \boldsymbol{\tau}^r_2 &= \mu\vartheta \begin{bmatrix} -\gamma_{12} \\ 1+\gamma_{11} \\ 0 \end{bmatrix} + \mu \begin{bmatrix} \gamma_{12} + \gamma_{21} \\ \gamma_{22} - \gamma_{11} \\ \gamma_{23} \end{bmatrix} \ , \end{aligned} \tag{77}$$

where

$$\vartheta = \vartheta(\bar{J}) = \frac{\lambda(\bar{J}^3 - 1) + 2\mu(\bar{J} - 1)}{\lambda\bar{J}^3 + 2\mu\bar{J}} \ . \tag{78}$$

Notice that $\boldsymbol{\tau}^r_\alpha \cdot \boldsymbol{e}^r_3 = \mu\gamma_{\alpha 3}$, and that $\gamma_{\alpha 3}$ do not appear in the expressions of the components $\tau^r_{\alpha\beta}$. Knowing $\boldsymbol{\tau}^r_\alpha$ from (77), it is then possible to compute the tangent tensors of (52), leading to

$$\bar{\boldsymbol{C}}_{11}=\mu\begin{bmatrix}(1+\gamma_{22})^2\vartheta'+1 & -(1+\gamma_{22})\gamma_{21}\vartheta' & 0\\ -(1+\gamma_{22})\gamma_{21}\vartheta' & \gamma_{21}^2\vartheta'+1 & 0\\ 0 & 0 & 1\end{bmatrix},$$

$$\bar{\boldsymbol{C}}_{12}=\mu\begin{bmatrix}-(1+\gamma_{22})\gamma_{12}\vartheta' & \vartheta-1+(1+\gamma_{11})(1+\gamma_{22})\vartheta' & 0\\ 1-\vartheta-\gamma_{12}\gamma_{21}\vartheta' & -(1+\gamma_{11})\gamma_{21}\vartheta' & 0\\ 0 & 0 & 0\end{bmatrix},$$

$$\bar{\boldsymbol{C}}_{21}=\bar{\boldsymbol{C}}_{12}^T \text{ and}$$

$$\bar{\boldsymbol{C}}_{22}=\mu\begin{bmatrix}\gamma_{12}^2\vartheta'+1 & -(1+\gamma_{11})\gamma_{12}\vartheta' & 0\\ -(1+\gamma_{11})\gamma_{12}\vartheta' & (1+\gamma_{11})^2\vartheta'+1 & 0\\ 0 & 0 & 1\end{bmatrix}, \tag{79}$$

in which

$$\vartheta'=\frac{(\lambda+2\mu)\left(3\lambda\bar{J}^2+2\mu\right)}{\bar{J}^2\left(\lambda\bar{J}^2+2\mu\right)^2}\ . \tag{80}$$

Remark 3
Up to first order in γ_α^r, we have from (77)

$$\boldsymbol{\tau}_\alpha^r=\bar{\boldsymbol{C}}_{\alpha\beta}\boldsymbol{\gamma}_\beta^r\ , \tag{81}$$

with

$$\bar{\boldsymbol{C}}_{11}=\begin{bmatrix}\bar{E} & 0 & 0\\ 0 & \mu & 0\\ 0 & 0 & \mu\end{bmatrix},\quad \bar{\boldsymbol{C}}_{12}=\begin{bmatrix}0 & \bar{E}\nu & 0\\ \mu & 0 & 0\\ 0 & 0 & 0\end{bmatrix},$$

$$\bar{\boldsymbol{C}}_{22}=\begin{bmatrix}\mu & 0 & 0\\ 0 & \bar{E} & 0\\ 0 & 0 & \mu\end{bmatrix} \tag{82}$$

and with $\bar{\boldsymbol{C}}_{21}=\bar{\boldsymbol{C}}_{12}^T$. Here the following material coefficients

$$\nu=\frac{1}{2}\frac{\lambda}{\lambda+\mu}\quad\text{and}\quad\bar{E}=\frac{2\mu}{1-\nu} \tag{83}$$

have been introduced. Although the linear material described by relation (81) is not affected by superimposed rigid body motions (and in this sense fulfills objectivity), it satisfies the local moment balance equation merely to first order in γ_α^r. It could be regarded as a small-strain large-displacement shell formulation, but the resulting model would depend on the mesh pattern up to first order in γ_α^r.

Remark 4
The often-used St.-Venant–Kirchhoff material has the following specific strain energy function (see e.g. [7])

$$\psi(\boldsymbol{E})=\frac{1}{2}\lambda(\boldsymbol{I}:\boldsymbol{E})^2+\mu(\boldsymbol{E}:\boldsymbol{E})\ . \tag{84}$$

From this expression, the second Piola–Kirchhoff stress tensor results in

$$\boldsymbol{S}=\lambda(\boldsymbol{I}:\boldsymbol{E})\boldsymbol{I}+2\mu\boldsymbol{E}\ , \tag{85}$$

while the tensor of the elastic tangent moduli is

$$\mathbb{D}=\lambda\boldsymbol{I}\otimes\boldsymbol{I}+2\mu\mathbb{I}\ . \tag{86}$$

Relation (85) may be conveniently rewritten as $\boldsymbol{S}=\mathbb{D}\boldsymbol{E}$, as one can show. Writing down the components of the Green–Lagrange strain tensor of (60) as

$$\begin{aligned}E_{\alpha\beta}&=\frac{1}{2}\left(\gamma_{\alpha\beta}+\gamma_{\beta\alpha}+\gamma_{\alpha\gamma}\gamma_{\beta\gamma}+\gamma_{\alpha3}\gamma_{\beta3}\right),\\ E_{\alpha3}&=\frac{1}{2}(1+\gamma_{33})\gamma_{\alpha3}\quad\text{and}\\ E_{33}&=\frac{1}{2}\left[(1+\gamma_{33})^2-1\right]\ ,\end{aligned} \tag{87}$$

then the plane stress condition of (56), along with (61), (83), (85) and (87), yields the following result for this material:

$$\gamma_{33}=\sqrt{1-\frac{2\nu}{1-\nu}\left(\gamma_{\alpha\alpha}+\frac{1}{2}\gamma_{\alpha\beta}\gamma_{\alpha\beta}\right)-\gamma_{\alpha3}\gamma_{\alpha3}}-1\ . \tag{88}$$

In addition, from $(66)_1$, (83) and (88) we may write

$$\boldsymbol{\tau}_1^r=\begin{bmatrix}\bar{E}(1+\gamma_{11})\left(E_{11}+\nu\left(E_{22}-\frac{1}{2}\gamma_{\alpha3}\gamma_{\alpha3}\right)\right)+2\mu\gamma_{21}E_{12}\\ 2\mu(1+\gamma_{22})E_{12}+\bar{E}\gamma_{12}\left(E_{11}+\nu\left(E_{22}-\frac{1}{2}\gamma_{\alpha3}\gamma_{\alpha3}\right)\right)\\ \mu\gamma_{13}+2\mu\gamma_{13}\left(E_{11}-\frac{1}{2}\gamma_{\alpha3}\gamma_{\alpha3}\right)+2\mu\gamma_{23}E_{12}\end{bmatrix}$$

and

$$\boldsymbol{\tau}_2^r=\begin{bmatrix}2\mu(1+\gamma_{11})E_{12}+\bar{E}\gamma_{21}\left(E_{22}+\nu\left(E_{11}-\frac{1}{2}\gamma_{\alpha3}\gamma_{\alpha3}\right)\right)\\ \bar{E}(1+\gamma_{22})\left(E_{22}+\nu\left(E_{11}-\frac{1}{2}\gamma_{\alpha3}\gamma_{\alpha3}\right)\right)+2\mu\gamma_{12}E_{12}\\ \mu\gamma_{23}+2\mu\gamma_{23}\left(E_{22}-\frac{1}{2}\gamma_{\alpha3}\gamma_{\alpha3}\right)+2\mu\gamma_{13}E_{12}\end{bmatrix}. \tag{89}$$

Notice the presence of $\gamma_{\alpha3}$ in the expressions of $\tau_{\alpha\beta}^r$. Furthermore the expressions of $\tau_{\alpha3}^r=\boldsymbol{\tau}_\alpha^r\cdot\boldsymbol{e}_3^r$ in (89) are much more complicated than those of (77). It is interesting to remark that the presenting plane-stress condition (i.e. on the first Piola–Kirchhoff stress) delivers $S_{33}=-\mu\gamma_{\alpha3}\gamma_{\alpha3}$, and not $S_{33}=0$ as commonly used in the literature. Moreover, despite its popularity, one should be aware that relation (84) is not poly-convex, and for that reason the solution of a boundary value problem with this specific strain energy function may actually not exist (see reference [7] for a detailed mathematical proof).

Incompressible isotropic materials
For incompressible isotropic elastic materials we state the strain energy function in the form $\psi=\psi(I_1,I_2)$, with $J=1$. The back-rotated first Piola–Kirchhoff stress tensor is then given by

$$\boldsymbol{P}^r=-p\boldsymbol{F}^{r-T}+2\boldsymbol{F}^r\left[\frac{\partial\psi}{\partial I_1}\boldsymbol{I}+\frac{\partial\psi}{\partial I_2}\boldsymbol{C}\right]\ , \tag{90}$$

where p is a hydrostatic pressure. Here, from $J=1$ in $(70)_1$ we have

$$\gamma_{33}=\frac{1}{\bar{J}}-1\ . \tag{91}$$

Although it represents an additional degree-of-freedom, p can be eliminated with the aid of the plane stress condition (56):

$$p = 2\bar{J}^{-2}\left[\frac{\partial\psi}{\partial I_1} + \frac{\partial\psi}{\partial I_2}\gamma_{\alpha 3}\gamma_{\alpha 3}\right] + 2\frac{\partial\psi}{\partial I_2}\bar{J}^{-4} \ . \tag{92}$$

As an example, the Neo–Hookean model of Treloar in [30, 31], given by

$$\psi(I_1) = \frac{1}{2}\mu(I_1 - 3) \ , \tag{93}$$

leads to

$$\boldsymbol{\tau}_1^r = \begin{bmatrix} \mu(\gamma_{11} - \gamma_{22}) + \mu(1 - \bar{J}^{-2})(1 + \gamma_{22}) \\ \mu(\gamma_{12} + \gamma_{21}) - \mu(1 - \bar{J}^{-2})\gamma_{21} \\ \mu\gamma_{13} \end{bmatrix} \quad \text{and}$$

$$\boldsymbol{\tau}_2^r = \begin{bmatrix} \mu(\gamma_{12} + \gamma_{21}) - \mu(1 - \bar{J}^{-2})\gamma_{12} \\ \mu(\gamma_{22} - \gamma_{11}) + \mu(1 - \bar{J}^{-2})(1 + \gamma_{11}) \\ \mu\gamma_{23} \end{bmatrix} \ . \tag{94}$$

in which (92) and (90) were applied.

4
The triangular shell finite element

We introduce an unconventional triangular shell element, from now on named T6-3i. The element is a 6-node displacement-based one, with a plane reference configuration as displayed in Fig. 2. A standard compatible quadratic displacement field $\boldsymbol{u}$ is placed on all nodes, while a linear interpolation scheme for the rotation vector $\boldsymbol{\theta}$ is set only on the mid-sides.

The absence of rotational degrees-of-freedom in the corner nodes makes the T6-3i a nonconforming element with respect to the rotation field, similarly to the ideas of [14] for linear plate triangles of the Reissner–Mindlin type. In reference [14], however, the concept of assumed strains is employed within a mixed formulation, and simple linear shape functions are used for the transversal displacements w and for the rotations θ_x and θ_y. Here, in contrast, we simply adopt higher order (quadratic) polynomials to

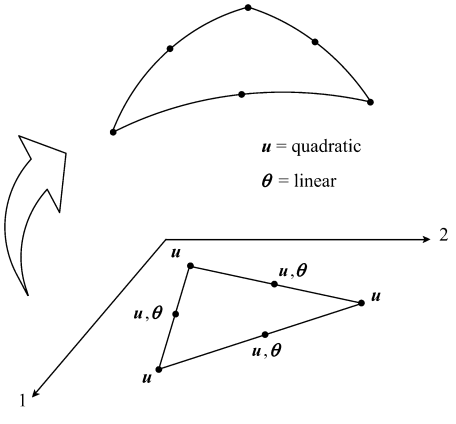

Fig. 2. The T6-3i element in reference and deformed configurations

interpolate the displacements $\boldsymbol{u}$, staying away of any expensive techniques such as mixed models with ANS or EAS. The T6-3i can this way enjoy all the simplicity and reliability of a pure displacement-based element, yet without any locking misbehavior.

As we work with the 3 components of the rotation vector, there is no need for special connection schemes on the shell edges and intersections. A fictitious stiffness of Eh^3 (E = elasticity modulus; h = shell thickness) is added to the drilling rotation locally at the element level, as this seems to be an optimal value (see [6]). This constitutes the only artificial numerical factor of our formulation.

We write the finite element interpolation in a particular element e, $e = 1, \ldots N_e$, as follows

$$\boldsymbol{d} = \mathbf{N}\mathbf{p}_e \ , \tag{95}$$

where $\mathbf{N}$ is the matrix of element shape functions and $\mathbf{p}_e$ the vector of element nodal displacements and rotations. The vector of the residual nodal forces for a particular element is then given by

$$\mathbf{P}_e = \int_{\Omega_e} \left[\mathbf{N}^T\bar{\boldsymbol{q}} - (\boldsymbol{\Psi}_\alpha\mathbf{N})^T\boldsymbol{\sigma}_\alpha\right]\mathrm{d}\Omega \ , \tag{96}$$

in which Ω_e is the element domain. The element tangent stiffness matrix is straightforwardly obtained with the help of (49), leading to

$$\mathbf{k}_e = \int_{\Omega_e} \left[(\boldsymbol{\Psi}_\alpha\mathbf{N})^T\boldsymbol{D}_{\alpha\beta}(\boldsymbol{\Psi}_\beta\mathbf{N}) + (\boldsymbol{\Delta}_\alpha\mathbf{N})^T\boldsymbol{G}_\alpha(\boldsymbol{\Delta}_\alpha\mathbf{N}) - \mathbf{N}^T\boldsymbol{L}\mathbf{N}\right]\mathrm{d}\Omega \ . \tag{97}$$

Here it is important to remark that the linearization stated in (49) can be performed either before or after discretization. Assemblage of the global residual forces and of the global tangent stiffness may be done as usual by

$$\mathbf{R} = \sum_{e=1}^{N_e}\mathbf{A}_e^T\mathbf{P}_e \quad \text{and} \quad \mathbf{K} = \sum_{e=1}^{N_e}\mathbf{A}_e^T\mathbf{k}_e\mathbf{A}_e \ , \tag{98}$$

respectively, where $\mathbf{A}_e$ is the connectivity matrix relating the element nodal DOFs $\mathbf{p}_e$ with the whole domain nodal DOFs $\mathbf{r}$, i.e.

$$\mathbf{p}_e = \mathbf{A}_e\mathbf{r} \ . \tag{99}$$

Equilibrium is then reached by vanishing the global residual forces,

$$\mathbf{R}(\mathbf{r}) = \boldsymbol{o} \ , \tag{100}$$

what can be iteratively solved by the Newton method for the free nodes.

Remark 5

It is valuable to point out that a lower-order version of the T6-3i, named T3-3i, was also implemented. The element is a triangle with linear interpolations for both displacements and rotations, yet compatible in the first and nonconforming in the latter. However, as expected for constant strain

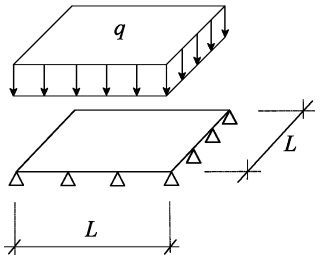

Fig. 3. Problem definition for Example 1

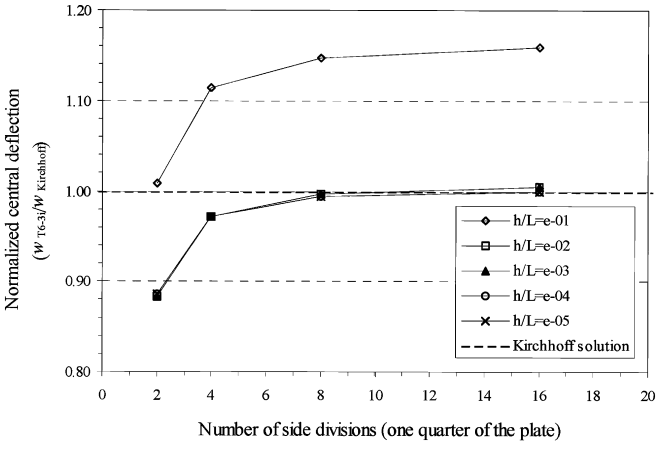

Fig. 4. Analysis results for Example 1

triangles, it performs quite well in plate-bending situations but displays a slightly poor in-plane response. Due to this the present work is restricted to the T6-3i only.

5
Numerical examples

In this section we assess the extent of our shell model together with the accuracy and reliability of the T6-3i element, by means of several numerical examples. For computation of the element matrices and vectors, 3 integration points – each one located on the element mid-sides – were adopted throughout. The material is assumed to be the neo-Hookean elastic isotropic of (73).

Example 1: Brief study of locking behaviour

This is a classical and illustrative test for locking investigation. A simply supported square plate is loaded by a uniform vertical pressure q, as shown in Fig. 3. Horizontal displacements in the 4 edges are assumed to be free, in order to avoid membrane stresses. The thickness of the plate is h and its length is $L = 2.0$ m, while the elasticity constants are adopted as $E = 10^6\,\mathrm{kN/m^2}$ and $\nu = 0.3$.

The intensity of the load is properly chosen for different values of the thickness, in a range from thick to very thin situations according with $q \sim h^3$ (see [5]). Figure 4 shows the central deflection w of the plate (normalized by Kirchhoff's analytical solution) versus the number of side divisions in one quarter of the structure, for T6-3i meshes with different ratios h/L. The non-locking behaviour is noticeable up to $h/L = 10^{-5}$. Similar results have been also

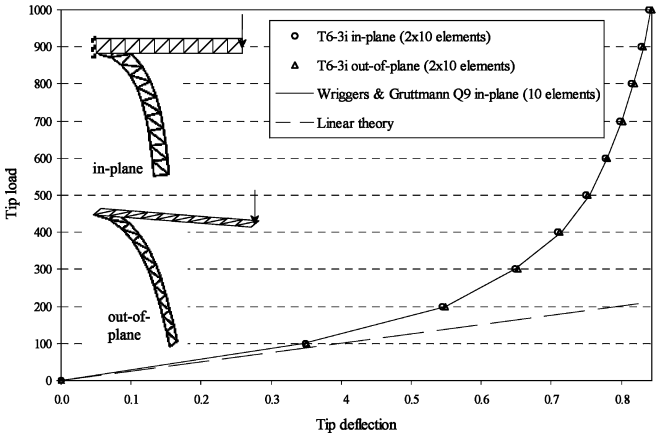

Fig. 5. Analysis results for Example 2

obtained for different plate geometries (rectangular, circular and skew)[2].

Example 2: Study of in-plane and out-of-plane behaviour

A cantilever beam of squared cross-section is subjected to a large point load at the center of its free end. With this simple example we want to show that the developed approach is capable to undergo large in-plane and out-of-plane rotations, as proposed in [24, 32]. The material is assumed to be of $E = 10^7$ and $\nu = 0.3$, while the beam dimensions are $L = 1.0$ and $b = h = 0.1$. Two different situations are enforced here: (i) in-plane bending with the load applied in the same plane of the beam and (ii) out-of-plane bending with the load applied in the out-of-plane direction. A plot of the load-deflection curve for the tip displacements is shown in Fig. 5, where almost identical results for both cases are found. Solution reported in [32] for Q9 quadrilateral Lagrangean elements with reduced integration is graphically indistinguishable. The deformed shapes are depicted in true scale.

Example 3: Lateral buckling of an L-shaped plate strip

The flat L-shaped plate strip of Fig. 6 is fully clamped in one edge and subjected to an in-plane point load at the free end. With $E = 71240\ \mathrm{N/mm^2}$ and $\nu = 0.31$, the lateral stability of the plate is here investigated as done in [1] for rod elements and in [24, 32] for shells. A very small perturbation load is imposed on the free edge in the out-of-plane direction, in order to initialize the post-critical lateral deflections. Fig. 7 shows the analysis results for a 2×68 T6-3i element mesh, where the deformed configuration at the last load step can also be seen in true scale. Our solution of $P_{cr} = 1.130$ is in good agreement with the values $P_{cr} = 1.128$ and $P_{cr} = 1.123$ reported in [24, 32] respectively.

Example 4: Ring plate loaded at free edge

This example was proposed in reference [2] and has been also analyzed by [4] and [32]. A circular ring plate with a

[2] The deflections displayed here are the linear solution of the problem, obtained after the first Newton iteration. Nonlinear results would be affected by membrane stresses, and therefore cannot be compared to the Kirchhoff's classical value of $w = 0.0443\,qL^4/Eh^3$. See [29]. We remark that the nonlinear results do not display locking effects either.

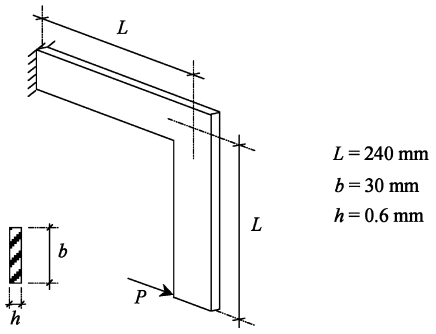

Fig. 6. Problem definition for Example 3

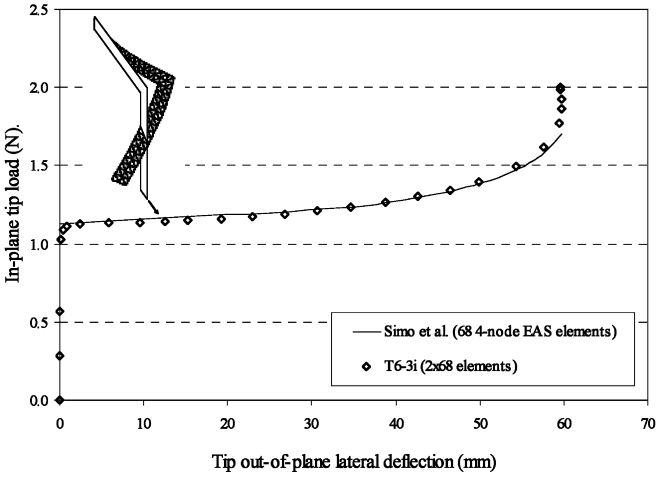

Fig. 7. Analysis results for Example 3

radial rip is loaded along its free edge by $p = 0.1f$ kN/m, the other edge being fully clamped. The outer and inner radius of the plate are $R = 10.0$ m and $r = 6.0$ m, respectively, while the thickness is $h = 0.03$ m. The material properties are assumed to be $E = 2.1 \times 10^8$ kN/m^2 and $\nu = 0$. Analyses were carried out with three T6-3i element meshes of the same pattern, differing from each other only on the degree of refinement (each finer mesh is embedded in the coarser). Vertical displacements $\boldsymbol{u}$ obtained for points A, B and C are plotted versus the load factor f on the next figures. As it can be seen, the results presented herein converge properly to the ones reported in the literature as the mesh is refined (for the sake of clearness only the curves from [4] are shown on the graphs; the remainders are nearly identical).

Example 5: Pinched hemispherical shell

This benchmark problem (see [13] and [24] among others) is concerned with the analysis of a hemispherical shell, with an 18° hole at one side, subjected to two inward and two outward symmetric forces 90° apart from each other as in Fig. 9. Symmetry conditions are used so that only one quadrant of the structure needs to be modeled. The material properties are taken as $E = 6.825 \times 10^7$ and $\nu = 0.3$, while the radius of the hemisphere is $R = 10.0$ and its thickness $t = 0.04$. In order to verify the large deformation capabilities of the formulation, the loads are increased by a factor of 100.

In Fig. 10 one can see the final deformed configuration for a typical T6-3i element mesh, without any magnification. Plots of the pinching load values versus the deflec-

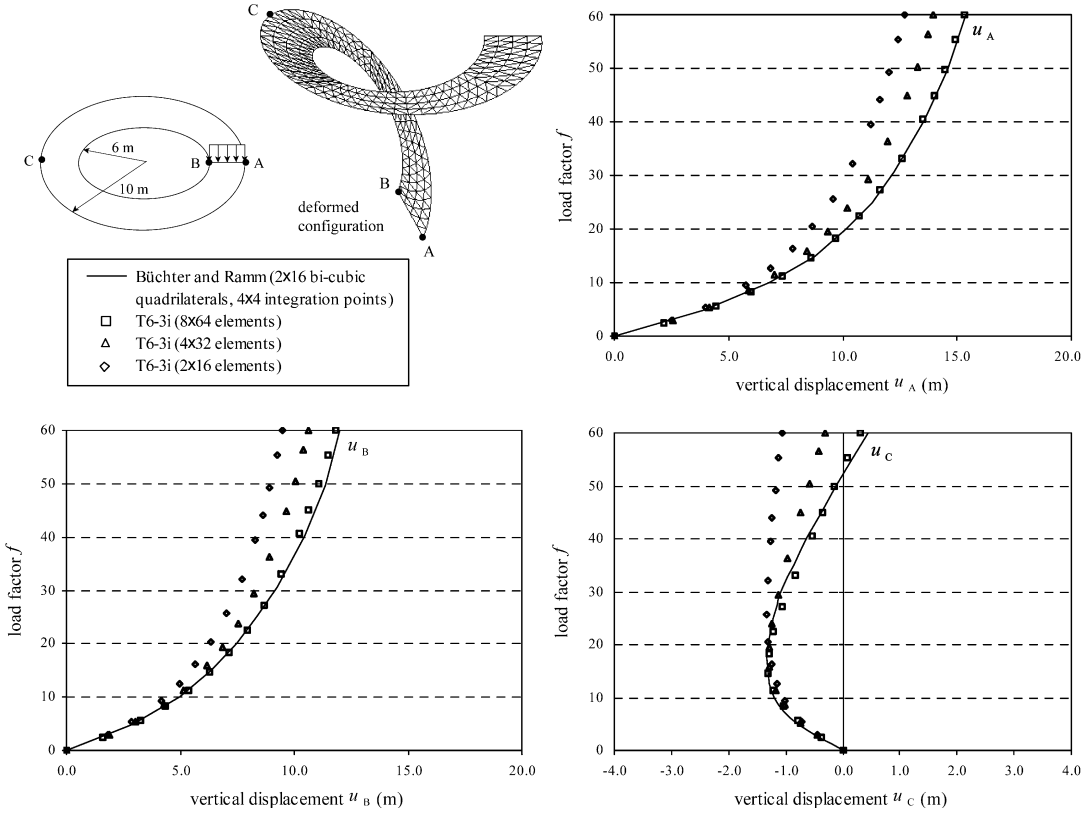

Fig. 8. Problem definition and analyses results for Example 4

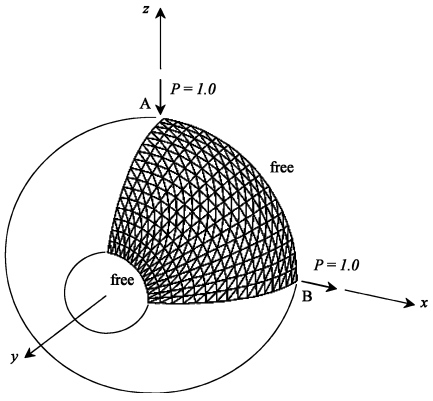

Fig. 9. Problem definition for Example 5

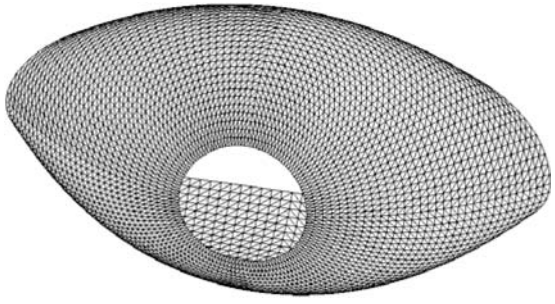

Fig. 10. Final deformed configuration for Example 5 (true scale)

tions of points A and B are shown in the sequence for different meshes.

Once more the results presented here converge appropriately to the ones reported in the literature, as the mesh is refined.

Example 6: Pull-out of an open cylinder

The open cylindrical shell of Fig. 12 is pulled by two diametrically opposite point forces P, the same as in [12], [16] and [28]. The material is assumed to have $E = 10.5 \times 10^6$ and $\nu = 0.3125$. One-eighth of the cylinder is modeled here by $2 \times 8 \times 16$ T6-3i elements, with the same mesh pattern as in references [16, 28]. Figure 13 shows the converged upward deflections of point A versus the pulling force P, and the final deformed configuration is depicted aside in true scale.

One should notice the slight snap-through behaviour of the solution when $P \approx 2.0 \times 10^4$, what also happens in the references mentioned.

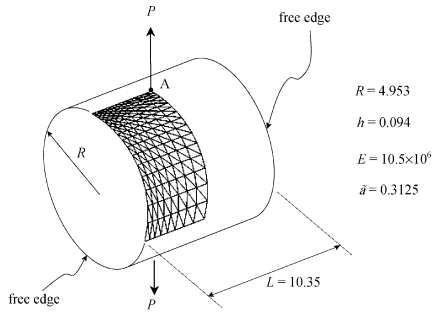

Fig. 12. Problem definition for Example 6

Example 7: Pinched cylinder

A cylindrical shell with rigid end-diaphragms is pinched by two opposite point loads as in Fig. 14, similarly to a finger-pinched beer can. The material properties of the cylinder are taken as $E = 3.0 \times 10^4$ and $\nu = 0$, and the pinching forces are increased up to $P = 12000$. For symmetry reasons only one octant of the can is modeled, with a $2 \times 32 \times 32$ T6-3i uniform mesh. Progression of the displacements at points A (in vertical direction) and B (in horizontal direction) are shown in Fig. 15, together with the solution from [23] in which enhanced strain elements were employed. The deformed configuration in true scale at the maximum load is portrayed next.

Concluding remarks

The shell model portrayed herein is reasonably simple and of great geometric appeal. Large rotations are exactly treated in the context of finite elasticity, and the plane stress condition as proposed here may render a very consistent approach for the implementation of elastoplastic constitutive models. Naturally, however, very large strain problems can be more realistically represented when thickness change is assumed within the shell kinematics, what is considered in detail in a next work [22]. At the moment, the T6-3i element presently introduced exhibits very promise results, with all the simplicity of a pure displacement-based finite element. A wide range of fully nonlinear problems from moderately thick to very thin shells can be regarded, yet without any expensive techniques such as ANS, EAS or hourglass control. General and reliable triangular shell elements combined with powerful mesh generators may constitute an excellent tool for nonlinear finite element analysis.

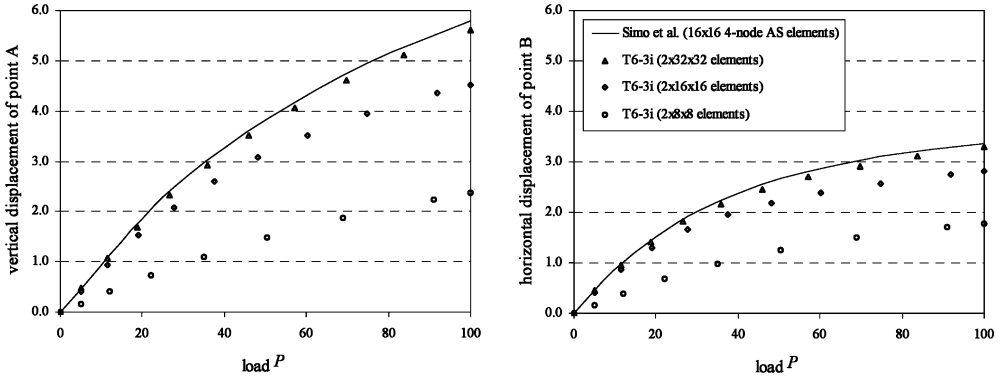

Fig. 11. Analysis results for Example 5

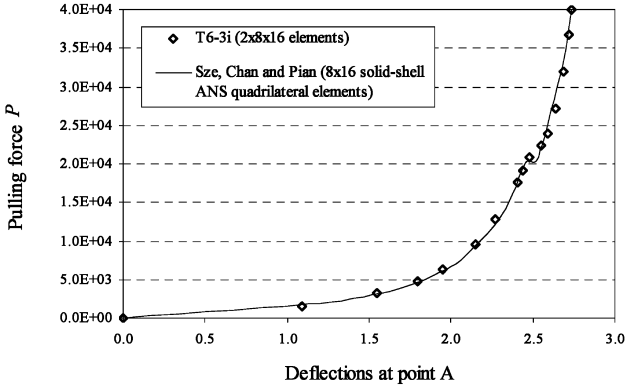

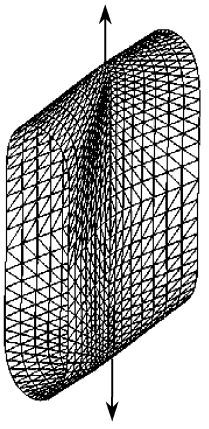

Fig. 13. Analysis results and final deformed configuration for Example 6

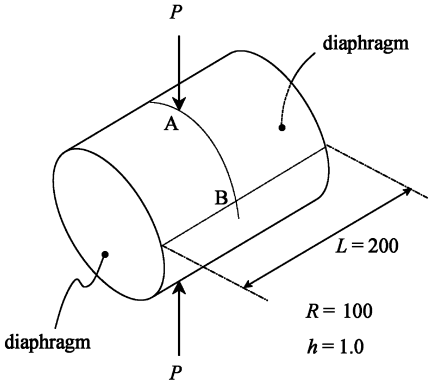

Fig. 14. Problem definition for Example 7

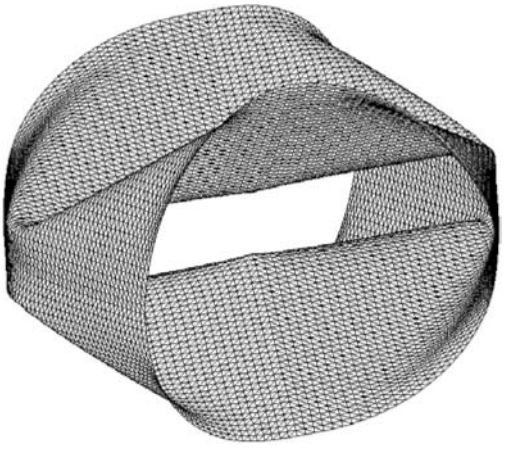

Fig. 16. Final deformed configuration for Example 7 (true scale)

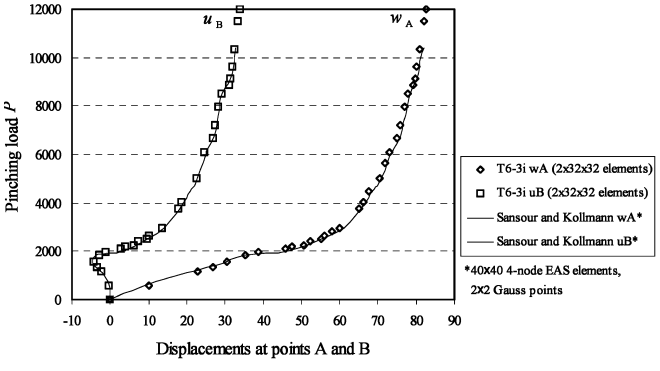

Fig. 15. Analysis results for Example 7

Appendix A: Alternative finite rotation parameters

A good number of different parameterizations is possible for the shell rotation field. For an instance, the quaternion rotation parameters (which are due to Hamilton) are defined by $\cos\theta$ and $\sin\theta\boldsymbol{e}$, in which $\boldsymbol{e} = (1/\theta)\boldsymbol{\theta}$ is the unit vector on the rotation axis (the proof of its existence is a celebrated theorem by Euler). In turn, the Rodrigues rotation parameters may be defined by

$$\boldsymbol{\alpha} = \alpha\boldsymbol{e}, \quad \text{where} \quad \alpha = 2\tan\frac{\theta}{2} \ . \tag{101}$$

Sometimes these parameters are defined without the factor 2 in $(101)_2$. However, definition as in (101) has the advantage of $\alpha = \theta$ up to second order. From (6), we arrive at the following alternative expression for the Euler–Rodrigues formula

$$\boldsymbol{Q} = \boldsymbol{I} + \frac{4}{4+\alpha^2}\left(\boldsymbol{A} + \frac{1}{2}\boldsymbol{A}^2\right) \ , \tag{102}$$

where $\boldsymbol{A} = \text{skew}(\boldsymbol{\alpha})$ (see [21]). Another expression for $\boldsymbol{Q}$ in terms of $\boldsymbol{A}$ is given by the so-called Cailey transform, viz.

$$\boldsymbol{Q} = \left(\boldsymbol{I} - \frac{1}{2}\boldsymbol{A}\right)^{-1}\left(\boldsymbol{I} + \frac{1}{2}\boldsymbol{A}\right) \ . \tag{103}$$

The two factors in (103) commute since they are coaxial.

If $\boldsymbol{\alpha}$ is regarded as a function of scalar variables, then the counterpart of (9) is

$$\boldsymbol{\kappa}_\alpha = \boldsymbol{\Xi}\boldsymbol{\alpha}_{,\alpha} \ , \tag{104}$$

where

$$\boldsymbol{\Xi} = \frac{4}{4+\alpha^2}\left(\boldsymbol{I} + \frac{1}{2}\boldsymbol{A}\right) \ . \tag{105}$$

This tensor has the property $\boldsymbol{\Xi}^T = \boldsymbol{Q}^T\boldsymbol{\Xi} = \boldsymbol{\Xi}\boldsymbol{Q}^T$, and thus $\boldsymbol{\Xi} = \boldsymbol{Q}^T\boldsymbol{\Xi}\boldsymbol{Q} = \boldsymbol{Q}\boldsymbol{\Xi}\boldsymbol{Q}^T$ also holds. Additional identities $\boldsymbol{\Xi}\boldsymbol{A} = \boldsymbol{A}\boldsymbol{\Xi} = \boldsymbol{Q} - \boldsymbol{I}$ and $\boldsymbol{\Xi}\boldsymbol{\alpha} = (4/(4+\boldsymbol{\alpha}^2))\boldsymbol{\alpha}$ can moreover be constructed. On the other hand, differentiation of $\boldsymbol{\Xi}$ with respect to the scalar variables Ξ renders

$$\boldsymbol{\Xi}_{,\alpha} = \frac{1}{2}\frac{4}{4+\alpha^2}\left(\boldsymbol{A}_{,\alpha} - \left(\boldsymbol{\alpha}\cdot\boldsymbol{\alpha}_{,\alpha}\right)\boldsymbol{\Xi}\right) \ . \tag{106}$$

The Rodrigues rotation parameters lead habitually to simpler and more efficient expressions, totally free of trigonometric functions. However, according to (101), if $\boldsymbol{\alpha}$ is used instead of $\boldsymbol{\theta}$ the rotation angle must be restricted to $-\pi < \theta < \pi$ (some updating scheme can be envisaged to make this restriction applicable only to a single increment).

Any tensor of the form

$$\boldsymbol{Q} = \boldsymbol{I} + \frac{b}{a^2+b^2}\,\mathrm{skew}(\boldsymbol{e}) + \left(1 - \frac{a}{a^2+b^2}\right)\mathrm{skew}^2(\boldsymbol{e}) \ , \tag{107}$$

where $\boldsymbol{e}$ is the unit vector along the rotation axis and $a^2 + b^2 = 1$, is actually a rotation tensor. Thus, many other parameterizations are possible. The Euler rotation vector corresponds to the obvious choice $a = \cos\theta$ and $b = \sin\theta$. The Rodrigues parameters (101) correspond to

$$a = 1 - \frac{2\alpha^2}{4+\alpha^2} \quad \text{and} \quad b = \frac{4\alpha}{4+\alpha^2} \ . \tag{108}$$

For example, a family of modified Rodrigues parameters can be generated by

$$\boldsymbol{\alpha}_n = \alpha_n \boldsymbol{e}, \quad \text{where} \quad \alpha_n = 2n\tan\frac{\theta}{2n}, \quad n = 1, 2, 3\ldots. \tag{109}$$

For $n = 1$ we recover (101). Notice that when $\boldsymbol{\alpha}_n$ is used the rotation angle must be restricted to $-n\pi < \theta < n\pi$. The counterparts of (102) and (103) for this family are

$$\boldsymbol{Q}^{1/n} = \boldsymbol{I} + \frac{4}{4n^2+\alpha_n^2}\left(n\boldsymbol{A}_n + \frac{1}{2}\boldsymbol{A}_n^2\right) \quad \text{and}$$
$$\boldsymbol{Q}^{1/n} = \left[\boldsymbol{I} - \frac{1}{2n}\boldsymbol{A}_n\right]^{-1}\left[\boldsymbol{I} + \frac{1}{2n}\boldsymbol{A}_n\right] \ , \tag{110}$$

respectively, where $\boldsymbol{A}_n = \mathrm{skew}(\boldsymbol{\alpha}_n)$. The two factors in $(110)_2$ commute since they are coaxial.

Appendix B: Geometric terms

The following result is obtained by differentiation

$$\frac{\partial\left(\boldsymbol{\Gamma}^T\boldsymbol{t}\right)}{\partial\boldsymbol{\theta}} = \boldsymbol{\Gamma}^T\frac{\partial\boldsymbol{t}}{\partial\boldsymbol{\theta}} + \boldsymbol{V}(\boldsymbol{\theta},\boldsymbol{t}) \ , \tag{111}$$

where $\boldsymbol{t}$ is a generic vector,

$$\begin{aligned}\boldsymbol{V}(\boldsymbol{\theta},\boldsymbol{t}) = {} & h_2(\theta)\boldsymbol{T} + h_3(\theta)(\boldsymbol{T}\boldsymbol{\Theta} - 2\boldsymbol{\Theta}\boldsymbol{T}) + \\ & - h_4(\theta)(\boldsymbol{\Theta}\boldsymbol{t}\otimes\boldsymbol{\theta}) + h_5(\theta)\left(\boldsymbol{\Theta}^2\boldsymbol{t}\otimes\boldsymbol{\theta}\right) \ ,\end{aligned} \tag{112}$$

and $\boldsymbol{T} = \mathrm{skew}(\boldsymbol{t})$. The tensor $\boldsymbol{V}(\boldsymbol{\theta},\boldsymbol{t})$ has the property

$$\boldsymbol{V}(\boldsymbol{\theta},\boldsymbol{t}) = \boldsymbol{V}^T(\boldsymbol{\theta},\boldsymbol{t}) + \boldsymbol{\Gamma}^T\boldsymbol{T}\boldsymbol{\Gamma} \ . \tag{113}$$

With the aid of (111) and (112), we can then obtain the derivatives

$$\begin{aligned}&\boldsymbol{G}_\alpha^{u'\theta} = \boldsymbol{G}_\alpha^{\theta u'T} = -\boldsymbol{N}_\alpha\boldsymbol{\Gamma}, \\ &\boldsymbol{G}_\alpha^{\theta\theta'} = \boldsymbol{G}_\alpha^{\theta'\theta T} = \boldsymbol{V}(\boldsymbol{\theta},\boldsymbol{m}_\alpha) \quad \text{and} \\ &\boldsymbol{G}_\alpha^{\theta\theta} = \boldsymbol{G}_\alpha^{\theta\theta T} = \boldsymbol{\Gamma}^T\boldsymbol{Z}_{,\alpha}\boldsymbol{N}_\alpha\boldsymbol{\Gamma} - \boldsymbol{V}\left(\boldsymbol{\theta},\boldsymbol{z}_{,\alpha}\times\boldsymbol{n}_\alpha\right) \\ &\qquad\qquad + \boldsymbol{V}_{,\alpha}\left(\boldsymbol{\theta},\boldsymbol{\theta}_{,\alpha},\boldsymbol{m}_\alpha\right) - \boldsymbol{\Gamma}_{,\alpha}^T\boldsymbol{M}_\alpha\boldsymbol{\Gamma} \ ,\end{aligned} \tag{114}$$

where $\boldsymbol{N}_\alpha = \mathrm{skew}\ (\boldsymbol{n}_\alpha)$, $\boldsymbol{M}_\alpha = \mathrm{skew}\ (\boldsymbol{m}_\alpha)$ and

$$\begin{aligned}&\boldsymbol{V}_{,\alpha}\left(\boldsymbol{\theta},\boldsymbol{\theta}_{,\alpha},\boldsymbol{m}_\alpha\right) \\ &= h_3(\theta)\left(\boldsymbol{M}_\alpha\boldsymbol{\Theta}_{,\alpha} - 2\boldsymbol{\Theta}_{,\alpha}\boldsymbol{M}_\alpha\right) \\ &\quad - h_4(\theta)\left(\boldsymbol{\Theta}_{,\alpha}\boldsymbol{m}_\alpha\otimes\boldsymbol{\theta} + \boldsymbol{\Theta}\boldsymbol{m}_\alpha\otimes\boldsymbol{\theta}_{,\alpha}\right) \\ &\quad + h_5(\theta)\left(\left(\boldsymbol{\Theta}_{,\alpha}\boldsymbol{\Theta} + \boldsymbol{\Theta}\boldsymbol{\Theta}_{,\alpha}\right)\boldsymbol{m}_\alpha\otimes\boldsymbol{\theta} + \boldsymbol{\Theta}^2\boldsymbol{m}_\alpha\otimes\boldsymbol{\theta}_{,\alpha}\right) \\ &\quad + \left(\boldsymbol{\theta}\cdot\boldsymbol{\theta}_{,\alpha}\right)\left[h_4(\theta)\boldsymbol{M}_\alpha + h_5(\theta)(\boldsymbol{M}_\alpha\boldsymbol{\Theta} - 2\boldsymbol{\Theta}\boldsymbol{M}_\alpha)\right] \\ &\quad + \left(\boldsymbol{\theta}\cdot\boldsymbol{\theta}_{,\alpha}\right)\left[-h_6(\theta)(\boldsymbol{\Theta}\boldsymbol{m}_\alpha\otimes\boldsymbol{\theta}) + h_7(\theta)\left(\boldsymbol{\Theta}^2\boldsymbol{m}_\alpha\otimes\boldsymbol{\theta}\right)\right] \ .\end{aligned}$$

Here the following trigonometric functions have been introduced

$$h_6(\theta) = \frac{h_3(\theta) - h_2(\theta) - 4h_4(\theta)}{\theta^2} \quad \text{and}$$
$$h_7(\theta) = \frac{h_4(\theta) - 5h_5(\theta)}{\theta^2} \ . \tag{115}$$

The corresponding results for the Rodrigues parameters (101) are

$$\frac{\partial\left(\boldsymbol{\Xi}^T\boldsymbol{t}\right)}{\partial\boldsymbol{\alpha}} = \boldsymbol{\Xi}^T\frac{\partial\boldsymbol{t}}{\partial\boldsymbol{\alpha}} + \boldsymbol{W}(\boldsymbol{\alpha},\boldsymbol{t}) \ , \tag{116}$$

where

$$\boldsymbol{W}(\boldsymbol{\alpha},\boldsymbol{t}) = -\frac{1}{2}\frac{4}{4+\alpha^2}\left(\boldsymbol{\Xi}^T\boldsymbol{t}\otimes\boldsymbol{\alpha} - \boldsymbol{T}\right) \ . \tag{117}$$

Notice the connection to (113):

$$\boldsymbol{W}(\boldsymbol{\alpha},\boldsymbol{t}) = \boldsymbol{W}^T(\boldsymbol{\alpha},\boldsymbol{t}) + \boldsymbol{\Xi}^T\boldsymbol{T}\boldsymbol{\Xi} \ . \tag{118}$$

The submatrices of $\boldsymbol{G}_\alpha$ are now expressed by

$$\begin{aligned}&\boldsymbol{G}_\alpha^{u'\alpha} = \boldsymbol{G}_\alpha^{\alpha u'T} = -\boldsymbol{N}_\alpha\boldsymbol{\Xi} \\ &\boldsymbol{G}_\alpha^{\alpha\alpha'} = \boldsymbol{G}_\alpha^{\alpha'\alpha T} = \boldsymbol{W}(\boldsymbol{\alpha},\boldsymbol{m}_\alpha) \\ &\boldsymbol{G}_\alpha^{\alpha\alpha} = \boldsymbol{G}_\alpha^{\alpha\alpha T} = \boldsymbol{\Xi}^T\boldsymbol{Z}_{,\alpha}\boldsymbol{N}_\alpha\boldsymbol{\Xi} - \boldsymbol{W}\left(\boldsymbol{\alpha},\boldsymbol{z}_{,\alpha}\times\boldsymbol{n}_\alpha\right) \\ &\qquad\qquad + \boldsymbol{W}_{,\alpha}\left(\boldsymbol{\alpha},\boldsymbol{\alpha}_{,\alpha},\boldsymbol{m}_\alpha\right) - \boldsymbol{\Xi}_{,\alpha}^T\boldsymbol{M}_\alpha\boldsymbol{\Xi} \ ,\end{aligned} \tag{119}$$

where

$$\begin{aligned}\boldsymbol{W}_{,\alpha}\left(\boldsymbol{\alpha},\boldsymbol{\alpha}_{,\alpha},\boldsymbol{m}_\alpha\right) = {} & -\frac{1}{2}\frac{4}{4+\alpha^2}\left(\boldsymbol{\Xi}_{,\alpha}^T\boldsymbol{m}_\alpha\otimes\boldsymbol{\alpha} + \boldsymbol{\Xi}^T\boldsymbol{m}_\alpha\otimes\boldsymbol{\alpha}_{,\alpha}\right) \\ & + \frac{1}{4}\left(\frac{4}{4+\alpha^2}\right)^2\left(\boldsymbol{\alpha}\cdot\boldsymbol{\alpha}_{,\alpha}\right)\left(\boldsymbol{\Xi}^T\boldsymbol{m}_\alpha\otimes\boldsymbol{\alpha} - \boldsymbol{M}_\alpha\right) \ .\end{aligned} \tag{120}$$

Appendix C: Derivatives of the external loading

Semi-tangential external moments are conservative moments characterized by the following time derivative

$$\dot{\bar{\boldsymbol{m}}} = \frac{1}{2}\boldsymbol{\omega}\times\bar{\boldsymbol{m}} \ . \tag{121}$$

For this type of loading the matrix $\boldsymbol{L}$ of (50) has the aspect

$$\boldsymbol{L} = \begin{bmatrix} \boldsymbol{O} & \boldsymbol{O} \\ \boldsymbol{O} & \mathrm{sym}(\boldsymbol{V}(\boldsymbol{\theta}, \bar{\boldsymbol{m}})) \end{bmatrix} . \tag{122}$$

In contrast, for a constant eccentric force $\bar{\boldsymbol{n}}$ whose moment is $\bar{\boldsymbol{m}} = \boldsymbol{s} \times \bar{\boldsymbol{n}}$ (with $\boldsymbol{s}$ as the eccentricity vector), $\boldsymbol{L}$ is given by

$$\boldsymbol{L} = \begin{bmatrix} \boldsymbol{O} & \boldsymbol{O} \\ \boldsymbol{O} & \boldsymbol{\Gamma}^T \mathrm{sym}(\boldsymbol{S}\bar{\boldsymbol{N}})\boldsymbol{\Gamma} + \mathrm{sym}(\boldsymbol{V}(\boldsymbol{\theta}, \bar{\boldsymbol{m}})) \end{bmatrix} , \tag{123}$$

where $\boldsymbol{S} = \mathrm{skew}(\boldsymbol{s})$ and $\bar{\boldsymbol{N}} = \mathrm{skew}(\bar{\boldsymbol{n}})$. The corresponding results for the Rodrigues parameters defined in (101) are

$$\begin{aligned} \boldsymbol{L} &= \begin{bmatrix} \boldsymbol{O} & \boldsymbol{O} \\ \boldsymbol{O} & \mathrm{sym}(\boldsymbol{W}(\boldsymbol{\alpha}, \bar{\boldsymbol{m}})) \end{bmatrix} \quad \text{and} \\ \boldsymbol{L} &= \begin{bmatrix} \boldsymbol{O} & \boldsymbol{O} \\ \boldsymbol{O} & \boldsymbol{\Xi}^T \mathrm{sym}(\boldsymbol{S}\bar{\boldsymbol{N}})\boldsymbol{\Xi} + \mathrm{sym}(\boldsymbol{W}(\boldsymbol{\alpha}, \bar{\boldsymbol{m}})) \end{bmatrix} . \end{aligned} \tag{124}$$

References

1. **Argyris JH, Balmer H, Doltsinis J St, Dunne PC, Haase M, Hasse M, Kleiber M, Malejannakis GA, Mlejenek HP, Muller M, Scharpf DW** (1979) Finite element method – The natural approach. Comput. Meth. Appl. Mech. Eng. 17/18: 1–106
2. **Basar Y, Ding Y** (1992) Finite rotation shell elements for the analysis of finite rotation shell problems. Int. J. Numer. Meth. Eng. 34: 165–169
3. **Betsch P, Gruttmann F, Stein E** (1996) A 4-node finite shell element for the implementation of general hyperelastic 3D-elasticity at finite strains. Comput. Meth. Appl. Mech. Eng. 130: 57–79
4. **Büchter N, Ramm E** (1992) Shell theory versus degeneration – a comparison in large rotation finite element analysis. Int. J. Numer. Meth. Eng. 34: 39–59
5. **Chapelle D, Bathe K-J** (1998) Fundamental considerations for the finite element analysis of shell structures. Comput. Struct. 66(1): 19–36
6. **Chroscielewski J, Makowski J, Stumpf H** (1992) Genuinely resultant shell finite elements accounting for geometric and material non-linearity. Int. J. Numer. Meth. Eng. 35: 63–94
7. **Ciarlet PJ** (1988) Mathematical Elasticity, v.1. North Holland, Amsterdam
8. **Dvorkin EN, Bathe K-J** (1984) A continuum mechanics based 4-node shell element for general nonlinear analysis. Eng. Comput. 1: 77–88
9. **Eberlein R, Wriggers P** (1999) Finite element concepts for finite elastoplastic strains and isotropic stress response in shells: theoretical and computational analysis. Comput. Meth. Appl. Mech. Eng. 17: 243–278
10. **Gruttmann F, Wagner W, Meyer L, Wriggers P** (1993) A nonlinear composite shell element with continuous interlaminar shear stresses. Comput. Mech. 13: 175–188
11. **Hughes TJR, Liu WK** (1981) Nonlinear finite element analysis of shells: Part I. Three-dimensional shells. Comput. Meth. Appl. Mech. Eng. 26: 331–362
12. **Jiang L, Chernuka MW** (1994) A simple four-noded corotational shell element for arbitrarily large rotations. Comput. Struct. 53: 1123–1132
13. **MacNeal RH, Harder RL** (1985) A proposed standard set of problems to test FE accuracy. Finite Elements in Analysis and Design 1: 3–20
14. **Oñate E, Zarate F, Flores F** (1994) A simple triangular element for thick and thin plate and shell analysis. Int. J. Numer. Meth. Eng. 37: 2569–2582
15. **Parish H** (1995) A continuum-based shell theory for nonlinear application. Int. J. Numer. Meth. Eng. 38: 1855–1883
16. **Park HC, Cho C, Lee SW** (1995) An efficient assumed-strain element model with 6 DOF per node for geometrically nonlinear shells. Int. J. Numer. Meth. Eng. 38: 4101–4122
17. **Pimenta PM** (1993) On a geometrically-exact finite-strain shell model. In: Proceedings of the 3rd Pan-American Congress on Applied Mechanics, III PACAM, São Paulo
18. **Pimenta PM** (1993) On a geometrically-exact finite-strain rod model. In: Proceedings of the 3rd Pan-American Congress on Applied Mechanics, III PACAM, São Paulo
19. **Pimenta PM, Yojo T** (1993) Geometrically-exact analysis of spatial frames. Applied Mechanics Reviews, ASME, New York, v.46, 11, 118–128
20. **Pimenta PM** (1996) Geometrically-exact analysis of initially curved rods. In: Advances in Computational Techniques for Structural Engineering, Edinburgh, U.K., v.1, 99–108
21. **Pimenta PM, Campello EMB** (2001) Geometrically nonlinear analysis of thin-walled space frames. Proceedings of the Second European Conference on Computational Mechanics, II ECCM, Cracow, Poland
22. **Pimenta PM, Campello EMB, Wriggers P** A fully non-linear multi-parameter shell formulation (to be published)
23. **Sansour C, Kollmann FG** (2000) Families of 4-node and 9-node finite elements for a finite deformation shell theory. An assessment of hybrid stress, hybrid strain and enhanced strain elements. Comput. Mech. 24: 435–447
24. **Simo JC, Fox DD, Rifai MS** (1990) On a stress resultant geometrically exact shell model. Part III: computational aspects of the nonlinear theory. Comput. Meth. Appl. Mech. Eng. 79: 21–70
25. **Simo JC, Hughes TRJ** (1991) Plasticity and viscoplasticity: Numerical analysis and computational aspects. Springer-Verlag, Berlin
26. **Stander N, Matzenmiller A, Ramm E** (1989) An assessment of assumed strain methods in finite rotation shell problems. Eng. Comput. 6: 58–66
27. **Steigmann DJ** (2002) Invariants of the stretch tensors and their application to finite elasticity theory. Mathematics and Mechanics of Solids 7: 393–404
28. **Sze KY, Chan WK, Pian THH** (2002) An 8-node hybrid-stress solid-shell element for geometric nonlinear analysis of elastic shells. Int. J. Numer. Meth. Eng. 55: 853–878
29. **Timoshenko SP, Woinowsky-Krieger** (1959) Theory of plates and shells. McGraw-Hill, New York
30. **Treloar LRG** (1943) The elasticity of a network of long chain molecules-I. Transactions of the Faraday Society 39: 36–41
31. **Treloar LRG** (1943) The elasticity of a network of long chain molecules-II. Transactions of the Faraday Society 39: 241–246
32. **Wriggers P, Gruttmann F** (1993) Thin shells with finite rotations formulated in Biot stresses: theory and finite element formultation. Int. J. Numer. Meth. Eng. 36: 2049–2071
33. **Wriggers P, Wagner W, Stein E** (1987) Algorithms for nonlinear contact constraints with application to stability problems of rods and shells. Comput. Mech. 2: 215–230